International Journal of Heat and Fluid Flow 70 (2018) 279–298

Contents lists available at ScienceDirect

International Journal of Heat and Fluid Flow

journal homepage: www.elsevier.com/locate/ijhff

A cascaded lattice Boltzmann model for thermal convective flows with local heat sources

Fatma M. Elseid, Samuel W.J. Welch*, Kannan N. Premnath

Department of Mechanical Engineering, University of Colorado Denver, Denver, CO 80217, United States

ARTICLE INFO

Keywords:
Lattice Boltzmann method
Convection diffusion equation
Central moments
Thermal flows

ABSTRACT

A cascaded central moment based lattice Boltzmann (LB) method for solving low Mach number thermal convective flows with source terms in two-dimensions in a double distribution function framework is presented. For the passive temperature field, which satisfies the convection diffusion equation (CDE) with a source term to represent internal/external local heat source, a new cascaded collision kernel is presented. Due to the use of a single conserved variable in the thermal energy equation, the cascaded structure in its collision operator begins from the first order moments and evolves to higher order moments. This is markedly different from the collision operator for the fluid flow equations, constructed in previous work, where the cascaded formulation starts at the second order moments in its collision kernel. A consistent implementation of the spatially and temporally varying source terms in the thermal cascaded LB method representing the heat sources in the CDE that maintains second order accuracy via a variable transformation is discussed. The consistency of the thermal cascaded LB method including a source term for the D2Q9 lattice with the macroscopic convection–diffusion equation is demonstrated by means of a Chapman–Enskog analysis. The new model is tested on a set of benchmark problems such as the thermal Poiseuille flow, thermal Couette flow with either wall injection or including viscous dissipation and natural convection in a square cavity. The validation study shows that the thermal cascaded LB method with source term is in very good agreement with the analytical solutions or numerical results reported for the benchmark problems. In addition, the numerical results show that our new thermal cascaded LB model maintains second order accuracy.

1. Introduction

The lattice-Boltzmann (LB) method is a kinetic theory based numerical method that has important features which make it attractive compared to the traditional numerical methods in the simulation of complex fluid flows and various other problems. While the latter involves direct discretization of the continuum equations, the LB approach is a macroscopic method based on the streaming and collision of the particle distribution functions. Some of the advantages of the LB method are its ability to incorporate kinetic models for complex fluids and flows, ease in dealing with complex boundary conditions and the property of locality of computation that enable simulation of large scale problems (Chen and Doolen, 1998; Aidun and Clausen, 2010; Succi, 2001; Guo and Shu, 2013; Krüger et al., 2017).

To simulate thermal convective flows, the solution of the temperature field, whose evolution is represented by a convection–diffusion equation (CDE), for the energy transport is coupled to the fluid velocity, which is represented by the Navier–Stokes (NS) equations. Classical numerical methods can become challenging to apply for the simulation of such flows, especially in complex geometries such as thermal flows in porous media. Within the LB framework, broadly, three different approaches that have been developed to construct the thermal lattice Boltzmann equation (LBE) equation models. These include (i) Multi-speed approach (MS-LBE) (Alexander et al., 1993; Gan et al., 2011), (ii) Hybrid approach (Lallemand and Luo, 2003; Mezrhab et al., 2004) and (iii) Double distribution function approach (DDF) (He et al., 1998; Shi et al., 2004; Mai et al., 2010; Chai and Zhao, 2014).

Briefly, the multi-speed approach uses the same distribution function to solve both the NS equations and the CDE by considering higher order velocity moments of the density distribution function via a large velocity set for the lattice. In the Hybrid approach, the LBE method is used to solve the flow field while any conventional numerical method such as a finite difference scheme is used to solve the energy equation. In the DDF approach, two separate distributions functions are employed, one for the flow field and the other one for the temperature field. The above three models have certain limitations. For example,

* Corresponding author.
E-mail addresses: Fatma.Elseid@ucdenver.edu (F.M. Elseid), Sam.Welch@ucdenver.edu (S.W.J. Welch), Kannan.Premnath@ucdenver.edu (K.N. Premnath).

https://doi.org/10.1016/j.ijheatfluidflow.2018.02.007
Received 29 September 2017; Received in revised form 9 February 2018; Accepted 11 February 2018
Available online 20 March 2018
0142-727X/

multi-speed models suffer from numerical instability, and are restricted to a limited temperature range and the treatment of boundary conditions with large discrete velocity set is difficult. The hybrid approach does not include terms such as viscous heat dissipation and compression work, and it just represents a compromised solution (Li et al., 2012). Unlike the above two models, many such limitations can be overcome by the DDF models (Guo et al., 2007; Li et al., 2012) and they have, hence, received significantly more attention recently.

Most of the developments related to the DDF-LBE methods considered single relaxation time (SRT) collisions models (Ponce Dawson et al., 1993; Guo et al., 2002; Van der Sman and Ernst, 2000; Chopard et al., 2009; Chai and Zhao, 2013). Various aspects relevant to the LBE for correct representation of the CDE for the temperature field were identified. For example, the choice of the equilibrium distribution function with nonlinear velocity terms was found to be important in this regard (Chopard et al., 2009). Concurrently, various boundary condition schemes for the DDF-LBE were developed (Ginzburg, 2005; Yoshida and Nagaoka, 2010; Zhang et al., 2012; Li et al., 2013; Khazaeli et al., 2013; Huang and Yong, 2015). However, the use of SRT collision models, though simple in structure and characterized by the relaxation of all modes at the same rate, is known to suffer from instability issues, particularly when the transport coefficients such as the fluid viscosity and thermal diffusivity become relatively small. This limits the ability to reach higher Reynolds or Peclet numbers. One possibility to address this issue is to consider using multi-relaxation time (MRT) models for DDF-LBE approach (Ginzburg, 2013; Rasin et al., 2005; Yoshida and Nagaoka, 2010; Li et al., 2013; Wang et al., 2013; Chai and Zhao, 2014). In the MRT model, the collision process is mapped onto the raw moment space through an orthogonal transformation matrix, where different moments can relax at different rates. By representing the relaxation times of the hydrodynamic and non-hydrodynamic moments, the stability of the MRT model can be significantly improved.

A further improvement is to consider another type of MRT model, in which the collision step is executed in terms of the relaxation of central moments, in which the particle velocities are shifted by the local fluid velocity. Such type of collision model in a moving frame of reference leads to a cascaded structure of the higher order moments in terms of those at lower orders following collision and hence is referred to as the cascaded LB method (Geier et al., 2006). This may shown to be equivalent to adopting a generalized local equilibrium in the rest or lattice frame of reference (Asinari, 2008). A second order scheme for implementation of the body forces in the cascaded LBE and its consistency to the NS equations was presented in our previous work (Premnath and Banerjee, 2009). More recently, detailed comparisons of various collision models and the superior stability characteristics of the MRT cascaded LBE was demonstrated by Geier et al. (2015) and Ning et al. (2016). Furthermore, a preconditioned formulation of the cascaded LBE to significantly improve the steady state convergence acceleration was presented by Hajabdollahi and Premnath (2017).

In our present investigation, we will construct a new cascaded LBE scheme for thermal convective flows in the DDF framework. We derive a cascaded collision operator for the evolution of the temperature field represented by the CDE with source term in two-dimensions on the two-dimensional nine velocity (D2Q9) lattice. Since the number of conserved variables for the CDE is different from that of the NS equations, the structure of the cascaded collision operator for the evolution of the temperature field constructed in this work is expected to be markedly different from that for the flow field developed in the prior investigation. In order to maintain generality of the resulting thermal cascaded LB scheme, we incorporate source terms representing locally spatially/temporally varying heat sources. In this regard, a variable transformation will be introduced to maintain second order accuracy (He et al., 1999). We will verify the consistency of the thermal cascaded LBE with the macroscopic CDE with source term by means of a Chapman–Enskog analysis. Finally, we will present a detailed numerical validation study of the cascaded LB formulation for thermal flows by comparisons against various benchmark problems. Recently, a three-dimensional version of this approach has been presented in Hajabdollahi and Premnath (2018).

This paper is structured as follows: Section 2 presents the derivation of the cascaded-LBM for the CDE representing the evolution of the temperature field. Here, the choice of the moment basis, continuous and discrete forms of central moments for equilibrium and sources, and an overview of the construction of the cascaded collision operator including the source terms to represent local internal heat generation using a variable transformation will be discussed. Details of the construction of the cascaded collision operator will be provided in Appendix A. A consistency analysis of the thermal cascaded LBE based on a Chapman–Enskog multiscale moment expansion is presented in Appendix B. Section 3 discusses the numerical results as part of the validation study of the thermal cascaded-LBE against various benchmark problems. Finally, a summary and conclusions arising from this work are presented in Section 4.

2. Cascaded lattice Boltzmann method for thermal convective flow

Our main goal in this investigation is to construct a cascaded LB model for the evolution of the temperature field represented by the following CDE with source term

$$\frac{\partial T}{\partial t} + \mathbf{u}\cdot\nabla T = \nabla\cdot(\alpha\nabla T) + G, \tag{1}$$

where α is the thermal diffusivity coefficient, $T = T(x, y, t)$ and $\mathbf{u} = \mathbf{u}(x, y, \mathbf{t})$ are local temperature and velocity field, respectively. In addition, $G = G(x, y, t)$ is the local source term arising, for example, due to internal heat generation or viscous dissipation. In general, thermal transport can be significantly influenced by the presence of internal heat generation, such as those related to nuclear or chemical reactions generating local heating effects. Viscous heating effects due to shear stresses is another example. All of these effects can be represented as a prescribed local source term $G(x, y, t)$ in the thermal transport equation. To handle such a general case, here we develop a new cascaded LB model with a source term, which can recover the macroscopic equation represented by the CDE given in Eq. (1) above with second order accuracy. In Eq. (1), the local velocity field $\mathbf{u} = \mathbf{u}(x, y, \mathbf{t})$ satisfies the Navier–Stokes equations (NSE) given by

$$\nabla\cdot\mathbf{u} = \mathbf{0}, \tag{2a}$$

$$\frac{\partial \mathbf{u}}{\partial t} + \mathbf{u}\cdot\nabla\mathbf{u} = -\frac{\mathbf{1}}{\rho}\nabla P + \nu\nabla^{\mathbf{2}}\mathbf{u} + \mathbf{F}, \tag{2b}$$

where p is the pressure, ν is the kinematic viscosity of the fluid, ρ is the reference density and $\mathbf{F} = \rho\mathbf{a}$ is the local external force field. The velocity field $\boldsymbol{u}$ to be used in Eq. (1) is considered to be known, and can be obtained by solving another cascaded LBE constructed in previous work (Geier et al., 2006; Premnath and Banerjee, 2009). In particular, the specific cascaded LBE with forcing term for obtaining the velocity field $\boldsymbol{u}$ can be coupled to the new cascaded for the CDE to be developed in this work. In such a double distribution function (DDF) formulation, we refer the reader to the cascaded LBE with forcing term for the flow field presented in Premnath and Banerjee (2009) to maintain brevity and focus here on the construction of the cascaded LBE to solve for the temperature field $T = T(x, y, t)$, whose evolution is represented by Eq. (1)

The overall procedure to develop a thermal cascaded LBE involves the following: (i) prescribe a suitable choice of an orthogonal moment basis for the lattice velocity set, (ii) specify formulations for the continuous central moments of the equilibrium and the source term and equate them to the corresponding discrete central moments involved in the cascaded LBE for the CDE, (iii) transform the various discrete central moments in terms of various corresponding raw moments by

using the binomial theorem and (iv) construct the collision kernel appearing in the cascaded collision operator for solving the CDE with a source term in the LB model.

First, we select a suitable moment basis for the two-dimensional, nine velocity (D2Q9) lattice. We consider the usual "bra" and the "ket" notations , i.e. $\langle . |$ and $| . \rangle$ to denote 9-dimensional row and column vectors, respectively. Then, we obtain the following nine non-orthogonal basis vectors obtained from monomials $e_{\alpha x}^m e_{\alpha y}^n$ at successively increasing orders:

$$\mathscr{T} = [|T\rangle, |e_{\alpha x}\rangle, |e_{\alpha y}\rangle, |e_{\alpha x}^2 + e_{\alpha y}^2\rangle, |e_{\alpha x}^2 - e_{\alpha y}^2\rangle, |e_{\alpha x}e_{\alpha y}\rangle, |e_{\alpha x}^2 e_{\alpha y}\rangle, |e_{\alpha x}e_{\alpha y}^2\rangle, |e_{\alpha x}^2 e_{\alpha y}^2\rangle], \tag{3}$$

where

$$\begin{aligned} |T\rangle &= (1, 1, 1, 1, 1, 1, 1, 1, 1)^\dagger, \\ |e_{\alpha x}\rangle &= (0, 1, 0, -1, 0, 1, -1, -1, 1)^\dagger, \\ |e_{\alpha y}\rangle &= (0, 0, 1, 0, -1, 1, 1, -1, -1)^\dagger. \end{aligned}$$

The above nominal set of basis vectors is then transformed into an equivalent *orthogonal* set of basis vectors by means of the standard Gram–Schmidt procedure arranged in the increasing order of moments:

$$\begin{aligned} |K_0\rangle &= |T\rangle, \quad |K_1\rangle = |e_{\alpha x}\rangle, \quad |K_2\rangle = |e_{\alpha y}\rangle, \\ |K_3\rangle &= 3|e_{\alpha x}^2 + e_{\alpha y}^2\rangle - 4|1\rangle, \quad |K_4\rangle = |e_{\alpha x}^2 - e_{\alpha y}^2\rangle, \quad |K_5\rangle = |e_{\alpha x}e_{\alpha y}\rangle, \\ |K_6\rangle &= -3|e_{\alpha x}^2 e_{\alpha y}\rangle + 2|e_{\alpha y}\rangle, \quad |K_7\rangle = -3|e_{\alpha x}e_{\alpha y}^2\rangle + 2|e_{\alpha x}\rangle, \\ |K_8\rangle &= 9|e_{\alpha x}^2 e_{\alpha y}^2\rangle - 6|e_{\alpha x}^2 + e_{\alpha y}^2\rangle + 4|1\rangle. \end{aligned}$$

By grouping the above set of vectors, we obtain an orthogonal transformation matrix $\mathscr{K}$ as

$$\mathscr{K} = [|K_0\rangle, |K_1\rangle, |K_2\rangle, |K_3\rangle, |K_4\rangle, |K_5\rangle, |K_6\rangle, |K_7\rangle, |K_8\rangle], \tag{4}$$

which can be explicitly written as

$$\mathscr{K} = \begin{bmatrix} 1 & 0 & 0 & -4 & 0 & 0 & 0 & 0 & 4 \\ 1 & 1 & 0 & -1 & 1 & 0 & 0 & 2 & -2 \\ 1 & 0 & 1 & -1 & -1 & 0 & 2 & 0 & -2 \\ 1 & -1 & 0 & -1 & 1 & 0 & 0 & -2 & -2 \\ 1 & 0 & -1 & -1 & -1 & 0 & -2 & 0 & -2 \\ 1 & 1 & 1 & 2 & 0 & 1 & -1 & -1 & 1 \\ 1 & -1 & 1 & 2 & 0 & -1 & -1 & 1 & 1 \\ 1 & -1 & -1 & 2 & 0 & 1 & 1 & 1 & 1 \\ 1 & 1 & -1 & 2 & 0 & -1 & 1 & -1 & 1 \end{bmatrix}. \tag{5}$$

Next, in order to construct a cascaded LB collision operator for representing the evaluation of the temperature field, we need to present the continuous moments of the equilibria and the source term. The continuous equilibrium central moments of order $(m + n)$ can be defined as

$$\hat{\Pi}_{x^m y^n}^{eq} = \int_{-\infty}^{\infty}\int_{-\infty}^{\infty} g^{\mathscr{M}T}(\xi_x - u_x)^m(\xi_y - u_y)^n d\xi_x d\xi_y \tag{6}$$

which yields

$$\begin{aligned} |\hat{\Pi}_{x^m y^n}^{eq}\rangle &= (\hat{\Pi}_0^{eq}, \hat{\Pi}_x^{eq}, \hat{\Pi}_y^{eq}, \hat{\Pi}_{xx}^{eq}, \hat{\Pi}_{yy}^{eq}, \hat{\Pi}_{xy}^{eq}, \hat{\Pi}_{xxy}^{eq}, \hat{\Pi}_{xyy}^{eq}, \hat{\Pi}_{xxyy}^{eq})^\dagger, \\ &= (T, 0, 0, c_s^2 T, c_s^2 T, 0, 0, 0, c_s^4 T)^\dagger. \end{aligned} \tag{7}$$

Here, the equilibrium distribution function $g^{\mathscr{M}T}$ is obtained by making an analogy with Maxwell–Boltzmann distribution function $f^{\mathscr{M}}\left(\rho, \vec{u}, \vec{\xi}\right)$ in the continuous velocity space $\vec{\xi}$ by replacing the density ρ with temperature T in our DDF formulation. That is,

$$g^{\mathscr{M}T} = \frac{T}{\rho} f^{\mathscr{M}}\left(\rho, \vec{u}, \vec{\xi}\right) \tag{8}$$

with

$$f^{\mathscr{M}}\left(\rho, \vec{u}, \vec{\xi}\right) = \frac{\rho}{2\pi c_s^2}\exp\left[-\frac{\left(\vec{\xi} - \vec{u}\right)^2}{2c_s^2}\right], \tag{9}$$

where c_s is the lattice speed of sound. Typically for the D2Q9 model we consider $c_s^2 = 1/3$.

Similarly, defining the continuous central moments of the source term of order $(m + n)$ due to $G = G(x, y, t)$ appearing in Eq. (1) as

$$\hat{\Gamma}_{x^m y^n} = \int_{-\infty}^{\infty}\int_{-\infty}^{\infty} \Delta g^{\mathscr{G}}(\xi_x - u_x)^m(\xi_y - u_y)^n d\xi_x d\xi_y \tag{10}$$

where $\Delta g^{\mathscr{G}}$ is the change in the distribution function due to source G. Since the source G is expected to influence only the lowest order (zeroth) moment, we can prescribe the following ansatz:

$$\begin{aligned} |\hat{\Gamma}_{x^m y^n}\rangle &= (\hat{\Gamma}_0, \hat{\Gamma}_x, \hat{\Gamma}_y, \hat{\Gamma}_{xx}, \hat{\Gamma}_{yy}, \hat{\Gamma}_{xy}, \hat{\Gamma}_{xxy}, \hat{\Gamma}_{xyy}, \hat{\Gamma}_{xxyy})^\dagger, \\ &= (G, 0, 0, 0, 0, 0, 0, 0, 0)^\dagger. \end{aligned} \tag{11}$$

By using the above central moments, our goal is to develop the collision operator and the source term of the cascaded LBE. We use the trapezoidal rule to evaluate the source term of the cascaded LBE to maintain second order accuracy:

$$\begin{aligned} g_\alpha(\vec{x} + \vec{e}_\alpha\delta_t, t + \delta_t) = g_\alpha(\vec{x}, t) + \Omega_\alpha(\vec{x}, t) \\ + \frac{1}{2}[S_\alpha(\vec{x}, t) + S_\alpha(\vec{x} + \vec{e}_\alpha, t + \delta_t)]. \end{aligned} \tag{12}$$

Here, the collision term Ω_α can be represented as $\Omega_\alpha \equiv \Omega_\alpha(\mathbf{g}, \hat{\mathbf{h}}) = (\mathscr{K}\cdot\hat{\mathbf{h}})_\alpha$, where $\mathbf{g} \equiv |g_\alpha\rangle = (g_0, g_1, ..., g_8)^\dagger$ is the vector of distribution functions and $\hat{\mathbf{h}} \equiv |\hat{h}_\alpha\rangle = (\hat{h}_0, \hat{h}_1, ..., \hat{h}_8)^\dagger$ is a vector representing the collision kernel which will be developed later. The discrete form of the source term S_α in the cascaded LBE given above represents the influence of the local heat source G in the velocity space and is defined as $\mathbf{S} \equiv |S_\alpha\rangle = (S_0, S_1, S_2, ..., S_8)^\dagger$. Noting that Eq. (12) is semi-implicit, by using the standard variable transformation $\overline{g} = g_\alpha - \frac{1}{2}S_\alpha$ (He et al., 1999), the implicitness can be effectively removed. This yields

$$\overline{g}_\alpha(\vec{x} + \vec{e}_\alpha\delta_t, t + \delta_t) = \overline{g}_\alpha(\vec{x}, t) + \Omega_\alpha(\vec{x}, t) + S_\alpha(\vec{x}, t), \tag{13}$$

which maintains second order accuracy in an effectively time explicit method.

In order to obtain the expressions for the structure of the cascaded collision operator $\hat{\mathbf{h}}$ and the source terms $\mathbf{S}_\alpha$ in the presence of a spatially and/or temporally varying local heat source G, i.e. $G = G(x, y, t)$, we define the following set of discrete central moments.

$$\hat{\kappa}_{x^m y^n} = \sum_\alpha g_\alpha(e_{\alpha x} - u_x)^m(e_{\alpha y} - u_y)^n, \tag{14a}$$

$$\hat{\kappa}_{x^m y^n}^{eq} = \sum_\alpha g_\alpha^{eq}(e_{\alpha x} - u_x)^m(e_{\alpha y} - u_y)^n, \tag{14b}$$

$$\hat{\overline{\kappa}}_{x^m y^n} = \sum_\alpha \overline{g}_\alpha(e_{\alpha x} - u_x)^m(e_{\alpha y} - u_y)^n. \tag{14c}$$

$$\hat{\sigma}_{x^m y^n} = \sum_\alpha S_\alpha(e_{\alpha x} - u_x)^m(e_{\alpha y} - u_y)^n. \tag{14d}$$

We then match the discrete central moments of the distribution functions and source terms with the corresponding continuous central moments at each order, i.e.

$$\hat{\kappa}^{eq}_{x^m y^n} = \hat{\Pi}^{\mathscr{M}}_{x^m y^n}, \tag{15a}$$

$$\hat{\sigma}_{x^m y^n} = \hat{\Gamma}^{F}_{x^m y^n}. \tag{15b}$$

Thus, we obtain

$$|\hat{\kappa}^{eq}_{x^m y^n}\rangle = (\hat{\kappa}^{eq}_0, \hat{\kappa}^{eq}_x, \hat{\kappa}^{eq}_y, \hat{\kappa}^{eq}_{xx}, \hat{\kappa}^{eq}_{yy}, \hat{\kappa}^{eq}_{xy}, \hat{\kappa}^{eq}_{xxy}, \hat{\kappa}^{eq}_{xyy}, \hat{\kappa}^{eq}_{xxyy})^{\dagger}, = (T, 0, 0, c_s^2 T, c_s^2 T, 0, 0, 0, c_s^4 T)^{\dagger}. \tag{16}$$

$$|\hat{\sigma}_{x^m y^n}\rangle = (\hat{\sigma}_0, \hat{\sigma}_x, \hat{\sigma}_y, \hat{\sigma}_{xx}, \hat{\sigma}_{yy}, \hat{\sigma}_{xy}, \hat{\sigma}_{xxy}, \hat{\sigma}_{xyy}, \hat{\sigma}_{xxyy})^{\dagger}, =(G, 0, 0, 0, 0, 0, 0, 0, 0)^{\dagger}. \tag{17}$$

Since the actual computations in the cascaded LBE are performed in terms of the various raw moments, we define the following set of discrete raw moments (denoted with a prime symbol):

$$\hat{\kappa}'_{x^m y^n} = \sum_{\alpha} g_\alpha e^m_{\alpha x} e^n_{\alpha y}, \tag{18a}$$

$$\hat{\kappa}'^{eq}_{x^m y^n} = \sum_{\alpha} g^{eq}_\alpha e^m_{\alpha x} e^n_{\alpha y}, \tag{18b}$$

$$\hat{\bar{\kappa}}'_{x^m y^n} = \sum_{\alpha} \bar{g}_\alpha e^m_{\alpha x} e^n_{\alpha y}. \tag{18c}$$

$$\hat{\sigma}'_{x^m y^n} = \sum_{\alpha} S_\alpha e^m_{\alpha x} e^n_{\alpha y}. \tag{18d}$$

By using Eqs. (14d), (17) and (18d) and the binomial theorem, we obtain the following sets of discrete raw moments for the source term at different orders:

$$\hat{\sigma}'_0 = \langle S_\alpha | T\rangle = G, \tag{19a}$$

$$\hat{\sigma}'_x = \langle S_\alpha | e_{\alpha x}\rangle = u_x G, \tag{19b}$$

$$\hat{\sigma}'_y = \langle S_\alpha | e_{\alpha y}\rangle = u_y G, \tag{19c}$$

$$\hat{\sigma}'_{xx} = \langle S_\alpha | e^2_{\alpha x}\rangle = u_x^2 G, \tag{19d}$$

$$\hat{\sigma}'_{yy} = \langle S_\alpha | e^2_{\alpha y}\rangle = u_y^2 G, \tag{19e}$$

$$\hat{\sigma}'_{xy} = \langle S_\alpha | e_{\alpha x} e_{\alpha y}\rangle = u_x u_y G, \tag{19f}$$

$$\hat{\sigma}'_{xxy} = \langle S_\alpha | e^2_{\alpha x} e_{\alpha y}\rangle = u_x^2 u_y G, \tag{19g}$$

$$\hat{\sigma}'_{xyy} = \langle S_\alpha | e_{\alpha x} e^2_{\alpha y}\rangle = u_x u_y^2 G, \tag{19h}$$

$$\hat{\sigma}'_{xxyy} = \langle S_\alpha | e^2_{\alpha x} e^2_{\alpha y}\rangle = u_x^2 u_y^2 G. \tag{19i}$$

In order to obtain the source terms in the velocity space, we first compute the source moments projected to the orthogonal moment space, i.e. $\hat{m}_\beta = \langle K_\beta | S_\alpha\rangle$, where $\beta = 0, 1, 2, ..., 8$

$$m_0 = \langle K_0 | S_\alpha\rangle = G, \tag{20a}$$

$$m_1 = \langle K_1 | S_\alpha\rangle = u_x G, \tag{20b}$$

$$m_2 = \langle K_2 | S_\alpha\rangle = u_y G, \tag{20c}$$

$$m_3 = \langle K_3 | S_\alpha\rangle = (3u_x^2 + 3u_y^2 - 4)G, \tag{20d}$$

$$m_4 = \langle K_4 | S_\alpha\rangle = (u_x^2 - u_y^2)G, \tag{20e}$$

$$m_5 = \langle K_5 | S_\alpha\rangle = u_x u_y G, \tag{20f}$$

$$m_6 = \langle K_6 | S_\alpha\rangle = (-3u_x^2 u_y + 2u_y)G, \tag{20g}$$

$$m_7 = \langle K_7 | S_\alpha\rangle = (-3u_x u_y^2 + 2u_x)G, \tag{20h}$$

$$m_8 = \langle K_8 | S_\alpha\rangle = (9u_x^2 u_y^2 - 6(u_x^2 + u_y^2) + 4)G. \tag{20i}$$

Since there is only one conserved scalar for the thermal transport equation, the components of the raw moments of sources $\hat{\sigma}'_{x^m y^n}$ are different from those appearing in the cascaded LBE for fluid flow with forcing terms (Premnath and Banerjee, 2009). Then, using $(\mathscr{K}\cdot\mathbf{S})_\alpha = (\hat{m}_0, \hat{m}_1, \hat{m}_2, ..., \hat{m}_8)^{\dagger}$ and inverting it by exploiting the orthogonality of $\mathscr{K}$, we get the following expressions for the source terms S_α in velocity space:

$$S_0 = \frac{1}{9}[m_0 - m_3 + m_8], \tag{21a}$$

$$S_1 = \frac{1}{36}[4m_0 + 6m_1 - m_3 + 9m_4 + 6m_7 - 2m_8], \tag{21b}$$

$$S_2 = \frac{1}{36}[4m_0 + 6m_2 - m_3 - 9m_4 + 6m_6 - 2m_8], \tag{21c}$$

$$S_3 = \frac{1}{36}[4m_0 - 6m_1 - m_3 + 9m_4 - 6m_7 - 2m_8], \tag{21d}$$

$$S_4 = \frac{1}{36}[4m_0 - 6m_2 - m_3 - 9m_4 - 6m_6 - 2m_8], \tag{21e}$$

$$S_5 = \frac{1}{36}[4m_0 + 6m_1 + 6m_2 + 2m_3 + 9m_5 - 3m_6 - 3m_7 + m_8], \tag{21f}$$

$$S_6 = \frac{1}{36}[4m_0 - 6m_1 + 6m_2 + 2m_3 - 9m_5 - 3m_6 + 3m_7 + m_8], \tag{21g}$$

$$S_7 = \frac{1}{36}[4m_0 - 6m_1 - 6m_2 + 2m_3 + 9m_5 + 3m_6 + 3m_7 + m_8], \tag{21h}$$

$$S_8 = \frac{1}{36}[4m_0 + 6m_1 - 6m_2 + 2m_3 - 9m_5 + 3m_6 - 3m_7 + m_8]. \tag{21i}$$

In addition, in order to construct the cascaded collision operator for the solution of the temperature field, we need the raw moments of the collision kernel of different orders, i.e. $\sum_\alpha (\mathscr{K}\cdot\hat{\mathbf{h}})_\alpha e^m_{\alpha x} e^n_{\alpha y} = \sum_\beta \langle K_\beta | e^m_{\alpha x} e^n_{\alpha y}\rangle \hat{h}_\beta$. Since the temperature field T is a collision invariant, it follows that $\hat{h}_0 = 0$. Using this and considering the orthogonal basis vector K_β in Eq. (4), we get

$$\sum_\alpha (\mathscr{K}\cdot\hat{\mathbf{h}})_\alpha = \sum_\beta \langle K_\beta | T\rangle \hat{h}_\beta = 0, \tag{22a}$$

$$\sum_\alpha (\mathscr{K}\cdot\hat{\mathbf{h}})_\alpha e_{\alpha x} = \sum_\beta \langle K_\beta | e_{\alpha x}\rangle \hat{h}_\beta = 6\hat{h}_1, \tag{22b}$$

$$\sum_\alpha (\mathscr{K}\cdot\hat{\mathbf{h}})_\alpha e_{\alpha y} = \sum_\beta \langle K_\beta | e_{\alpha y}\rangle \hat{h}_\beta = 6\hat{h}_2, \tag{22c}$$

$$\sum_\alpha (\mathscr{K}\cdot\hat{\mathbf{h}})_\alpha e^2_{\alpha x} = \sum_\beta \langle K_\beta | e^2_{\alpha x}\rangle \hat{h}_\beta = 6\hat{h}_3 + 2\hat{h}_4, \tag{22d}$$

$$\sum_\alpha (\mathscr{K}\cdot\hat{\mathbf{h}})_\alpha e^2_{\alpha y} = \sum_\beta \langle K_\beta | e^2_{\alpha y}\rangle \hat{h}_\beta = 6\hat{h}_3 - 2\hat{h}_4, \tag{22e}$$

$$\sum_\alpha (\mathscr{K}\cdot\hat{\mathbf{h}})_\alpha e_{\alpha x} e_{\alpha y} = \sum_\beta \langle K_\beta | e_{\alpha x} e_{\alpha y}\rangle \hat{h}_\beta = 4\hat{h}_5, \tag{22f}$$

$$\sum_\alpha (\mathscr{K}\cdot\hat{\mathbf{h}})_\alpha e^2_{\alpha x} e_{\alpha y} = \sum_\beta \langle K_\beta | e^2_{\alpha x} e_{\alpha y}\rangle \hat{h}_\beta = 4\hat{h}_2 - 4\hat{h}_6, \tag{22g}$$

$$\sum_\alpha (\mathscr{K}\cdot\hat{\mathbf{h}})_\alpha e_{\alpha x} e^2_{\alpha y} = \sum_\beta \langle K_\beta | e_{\alpha x} e^2_{\alpha y}\rangle \hat{h}_\beta = 4\hat{h}_1 - 4\hat{h}_7, \tag{22h}$$

$$\sum_{\alpha}(\mathscr{K}\cdot\hat{\mathbf{h}})_{\alpha}e_{\alpha x}^{2}e_{\alpha y}^{2} = \sum_{\beta}\langle K_{\beta}|e_{\alpha x}^{2}e_{\alpha y}^{2}\rangle\hat{h}_{\beta} = 8\hat{h}_{3} + 4\hat{h}_{8}. \tag{22i}$$

Notice that $\hat{h}_1 \neq \hat{h}_2 \neq 0$ in the present case, which differs from the cascaded LBE for fluid flow (Premnath and Banerjee, 2009). This difference arises from the fact that the cascaded LBE for the flow field has three collision invariants, i.e. mass and momentum, and hence its corresponding zeroth and first order collision kernels are zero; on the other hand, in the case of the cascaded LBE for the thermal transport equation, there is only one collision invariant, i.e. the temperature field, and therefore only its zeroth order collision kernel, i.e. $\hat{h}_0$, is zero. As a result of these differences the cascaded collision operator for the temperature field is markedly different from that for the flow field.

We now need to find the expressions of $\langle\overline{g}_{\alpha}|e_{\alpha x}^{m}e_{\alpha y}^{n}\rangle = \sum_{\alpha=0}^{8}\overline{g}_{\alpha}e_{\alpha x}^{m}e_{\alpha y}^{n}$ to proceed further. For the conserved basis vector, we have in terms of the collisional invariant $\sum_{\alpha=0}^{8}\overline{g}_{\alpha} = T - \frac{1}{2}G$, and for the non-conserved basis vectors we have

$$\hat{\kappa}_{x}^{'} = \sum_{\alpha=0}^{8}\overline{g}_{\alpha}e_{\alpha x} = \overline{g}_{1} - \overline{g}_{3} + \overline{g}_{5} - \overline{g}_{6} - \overline{g}_{7} + \overline{g}_{8}, \tag{23a}$$

$$\hat{\kappa}_{y}^{'} = \sum_{\alpha=0}^{8}\overline{g}_{\alpha}e_{\alpha y} = \overline{g}_{2} - \overline{g}_{4} + \overline{g}_{5} + \overline{g}_{6} - \overline{g}_{7} - \overline{g}_{8}, \tag{23b}$$

$$\hat{\kappa}_{xx}^{'} = \sum_{\alpha=0}^{8}\overline{g}_{\alpha}e_{\alpha x}^{2} = \overline{g}_{1} + \overline{g}_{3} + \overline{g}_{5} + \overline{g}_{6} + \overline{g}_{7} + \overline{g}_{8}, \tag{23c}$$

$$\hat{\kappa}_{yy}^{'} = \sum_{\alpha=0}^{8}\overline{g}_{\alpha}e_{\alpha y}^{2} = \overline{g}_{2} + \overline{g}_{4} + \overline{g}_{5} + \overline{g}_{6} + \overline{g}_{7} + \overline{g}_{8}, \tag{23d}$$

$$\hat{\kappa}_{xy}^{'} = \sum_{\alpha=0}^{8}\overline{g}_{\alpha}e_{\alpha x}e_{\alpha y} = \overline{g}_{5} - \overline{g}_{6} + \overline{g}_{7} - \overline{g}_{8}, \tag{23e}$$

$$\hat{\kappa}_{xxy}^{'} = \sum_{\alpha=0}^{8}\overline{g}_{\alpha}e_{\alpha x}^{2}e_{\alpha y} = \overline{g}_{5} + \overline{g}_{6} - \overline{g}_{7} - \overline{g}_{8}, \tag{23f}$$

$$\hat{\kappa}_{xyy}^{'} = \sum_{\alpha=0}^{8}\overline{g}_{\alpha}e_{\alpha x}e_{\alpha y}^{2} = \overline{g}_{5} - \overline{g}_{6} - \overline{g}_{7} + \overline{g}_{8}, \tag{23g}$$

$$\hat{\kappa}_{xxyy}^{'} = \sum_{\alpha=0}^{8}\overline{g}_{\alpha}e_{\alpha x}^{2}e_{\alpha y}^{2} = \overline{g}_{5} + \overline{g}_{6} + \overline{g}_{7} + \overline{g}_{8} \tag{23h}$$

Now, we are in a position to determine the structure of the cascaded collision operator with source terms to solve for the thermal transport equation represented by the CDE. The procedure can be briefly summarized as follows: Starting from the lowest order non-conserved post-collision central moments (i.e. the first order components in the present case), we tentatively set them equal to their corresponding equilibrium states. Once the expressions for the collision kernel $\hat{h}_{\beta}$ ($\beta \geq 1$) is determined, we discard the equilibrium assumption and multiply it with a corresponding relaxation parameter λ_{β} to allow for a relaxation process during collision (Geier et al., 2006; Premnath and Banerjee, 2009). The details of the various intermediate steps involved in the derivation of the collision kernel are presented in Appendix A. In addition, as in Meng and Guo (2015), in order to maintain additional flexibility in the representation of the emergent transport coefficient (i.e. the thermal diffusivity of the CDE), we also introduce extended moment equilibria involving temperature gradient terms with an adjustable coefficient D, which acts as an effective relaxation parameter, in the first order equilibrium moments. The resulting final expressions of the collision kernel are given as follows:

$$\hat{h}_{0} = 0, \tag{24a}$$

$$\hat{h}_{1} = \frac{\lambda_{1}}{6}\left\{u_{x}T - \hat{\kappa}_{x}^{'} - \frac{1}{2}\hat{\sigma}_{x}^{'} + \frac{1}{3}D\delta t\left(\partial_{x}T\right)\right\}, \tag{24b}$$

$$\hat{h}_{2} = \frac{\lambda_{2}}{6}\left\{u_{y}T - \hat{\kappa}_{y}^{'} - \frac{1}{2}\hat{\sigma}_{y}^{'} + \frac{1}{3}D\delta t\left(\partial_{y}T\right)\right\}, \tag{24c}$$

$$\hat{h}_{3} = \frac{\lambda_{3}}{12}\left\{\frac{2}{3}T - (u_{x}^{2}+u_{y}^{2})T - \left(\hat{\kappa}_{xx}^{'} + \hat{\kappa}_{yy}^{'}\right) + 2u_{x}\hat{\kappa}_{x}^{'} + 2u_{y}\hat{\kappa}_{y}^{'} + \frac{1}{2}(\hat{\sigma}_{xx}^{'} + \hat{\sigma}_{yy}^{'})\right\} + u_{x}\hat{h}_{1} + u_{y}\hat{h}_{2}, \tag{24d}$$

$$\hat{h}_{4} = \frac{\lambda_{4}}{4}\left\{-(u_{x}^{2}-u_{y}^{2})T - \left(\hat{\kappa}_{xx}^{'} - \hat{\kappa}_{yy}^{'}\right) + 2u_{x}\hat{\kappa}_{x}^{'} - 2u_{y}\hat{\kappa}_{y}^{'} + \frac{1}{2}(\hat{\sigma}_{xx}^{'} - \hat{\sigma}_{yy}^{'})\right\} + 3u_{x}\hat{h}_{1} - 3u_{y}\hat{h}_{2}, \tag{24e}$$

$$\hat{h}_{5} = \frac{\lambda_{5}}{4}\left\{-u_{x}u_{y}T - \hat{\kappa}_{xy}^{'} + u_{x}\hat{\kappa}_{y}^{'} + u_{y}\hat{\kappa}_{x}^{'} + \frac{1}{2}\hat{\sigma}_{xy}^{'}\right\} + \frac{3}{2}(u_{x}\hat{h}_{2} + u_{y}\hat{h}_{1}), \tag{24f}$$

$$\hat{h}_{6} = \frac{\lambda_{6}}{4}\left\{-u_{x}^{2}u_{y}T + \hat{\kappa}_{xxy}^{'} - u_{y}\hat{\kappa}_{xx}^{'} - 2u_{x}\hat{\kappa}_{xy}^{'} + u_{y}^{2}\hat{\kappa}_{y}^{'} + 2u_{x}u_{y}\hat{\kappa}_{x}^{'} + \frac{1}{2}\hat{\sigma}_{xxy}^{'}\right\} + 3u_{x}u_{y}\hat{h}_{1} + \left(1 + \frac{3}{2}u_{x}^{2}\right)\hat{h}_{2} - \frac{3}{2}u_{y}\hat{h}_{3} - \frac{1}{2}u_{y}\hat{h}_{4} - 2u_{x}\hat{h}_{5}, \tag{24g}$$

$$\hat{h}_{7} = \frac{\lambda_{7}}{4}\left\{-u_{x}u_{y}^{2}T + \hat{\kappa}_{xyy}^{'} - u_{x}\hat{\kappa}_{yy}^{'} - 2u_{y}\hat{\kappa}_{xy}^{'} + 2u_{x}u_{y}\hat{\kappa}_{y}^{'} + u_{y}^{2}\hat{\kappa}_{x}^{'} + \frac{1}{2}\hat{\sigma}_{xyy}^{'}\right\} + \left(1 + \frac{3}{2}u_{y}^{2}\right)\hat{h}_{1} + 3u_{x}u_{y}\hat{h}_{2} - \frac{3}{2}u_{x}\hat{h}_{3} + \frac{1}{2}u_{x}\hat{h}_{4} - 2u_{y}\hat{h}_{5}, \tag{24h}$$

$$\hat{h}_{8} = \frac{\lambda_{8}}{4}\left\{\frac{1}{9}T - u_{x}^{2}u_{y}^{2}T - \hat{\kappa}_{xxyy}^{'} + 2u_{x}\hat{\kappa}_{xyy}^{'} + 2u_{y}\hat{\kappa}_{xxy}^{'} - u_{x}^{2}\hat{\kappa}_{yy}^{'} - u_{y}^{2}\hat{\kappa}_{xx}^{'} - 4u_{x}u_{y}\hat{\kappa}_{xy}^{'} + 2u_{x}u_{y}^{2}\hat{\kappa}_{x}^{'} + 2u_{x}^{2}u_{y}\hat{\kappa}_{y}^{'} + \frac{1}{2}\hat{\sigma}_{xxyy}^{'}\right\} + (2u_{x} + 3u_{x}u_{y}^{2})\hat{h}_{1} + (2u_{y} + 3u_{x}^{2}u_{y})\hat{h}_{2} - \left(2 + \frac{3}{2}u_{x}^{2} + \frac{3}{2}u_{y}^{2}\right)\hat{h}_{3} + \frac{1}{2}(u_{x}^{2} - u_{y}^{2})\hat{h}_{4} - 4u_{x}u_{y}\hat{h}_{5} - 2u_{y}\hat{h}_{6} - 2u_{x}\hat{h}_{7}. \tag{24i}$$

where, λ_{β}, $\beta = 1, 2, 3, \ldots, 8$, are the relaxation parameters, satisfying the bounds $0 < \lambda_{\beta} < 2$. Notice the cascaded structure for the second and higher order moment kernels, i.e. their dependence on the lower order moments for our thermal cascaded LBE. By contrast, the cascaded LBE for the fluid flow is significantly different, with the cascaded structure appearing only for third and higher order moments. When a Chapman–Enskog expansion (C–E) is performed on the above cascaded LB model (see Appendix B for details), it can be shown to recover the convection–diffusion thermal transport equation, with the relaxation parameters for the first order moments λ_1 and λ_2 and the adjustable coefficient D controlling the thermal diffusivity coefficient α (see Eq. (1)):

$\alpha = \frac{1}{3}\left(\frac{1}{\lambda_j} - \frac{1}{2} - D\right)\delta t$, $j = 1, 2$. The rest of the parameters can be adjusted independently to improve numerical stability. In this work, $\lambda_1 = \lambda_2$ is selected based on the specified diffusivity, while the remaining relaxation parameters are set to be unity. It may be noted that $1/\lambda_j - D$ for $j = 1, 2$. may be treated as an effective relaxation parameter.

Moreover, the temperature gradients $\partial_x T$ and $\partial_y T$ appearing in the above (see Eqs. (24b) and (24c)) can be calculated locally in terms of the first order non-equilibrium moments (see the C–E analysis given in Appendix B for details). Thus, we have

$$\frac{\partial T}{\partial x} = \frac{-3\lambda_1\left(\hat{\kappa}_x^{'} - \hat{\kappa}_x^{'eq}\right)}{(1 - D\lambda_1)}, \tag{25a}$$

$$\frac{\partial T}{\partial y} = \frac{-3\lambda_2\left(\hat{\kappa}_y^{'} - \hat{\kappa}_y^{'eq}\right)}{(1 - D\lambda_2)} \tag{25b}$$

where $\hat{\kappa}_x^{'} = \sum_{\alpha=0}^{8} e_{\alpha x}\overline{g}_\alpha$, $\hat{\kappa}_y^{'} = \sum_{\alpha=0}^{8} e_{\alpha y}\overline{g}_\alpha$, $\hat{\kappa}_x^{eq'} = u_x T$, and $\hat{\kappa}_y^{eq'} = u_y T$. Then, the thermal cascaded LBE given in Eq. (13) can be written in terms of the following collision and streaming steps:

$$\overline{g}_\alpha^p(\vec{x}, t) = \overline{g}_\alpha(\vec{x}, t) + \Omega_\alpha(\vec{x}, t) + S_\alpha(\vec{x}, t), \tag{26a}$$

$$\overline{g}_\alpha(\vec{x} + \vec{e}_\alpha, t + 1) = \overline{g}_\alpha^p(\vec{x}, t). \tag{26b}$$

By expanding $(\mathscr{K}\cdot\hat{\mathbf{h}})_\alpha$ in $\Omega_\alpha(\vec{x}, t)$ the explicit expressions for the post-collision distribution functions are given as follows:

$$\overline{g}_0^p = \overline{g}_0 + [\hat{h}_0 - 4(\hat{h}_3 - \hat{h}_8)] + S_0, \tag{27a}$$

$$\overline{g}_1^p = \overline{g}_1 + [\hat{h}_0 + \hat{h}_1 - \hat{h}_3 + \hat{h}_4 + 2(\hat{h}_7 - \hat{h}_8)] + S_1, \tag{27b}$$

$$\overline{g}_2^p = \overline{g}_2 + [\hat{h}_0 + \hat{h}_2 - \hat{h}_3 - \hat{h}_4 + 2(\hat{h}_6 - \hat{h}_8)] + S_2, \tag{27c}$$

$$\overline{g}_3^p = \overline{g}_3 + [\hat{h}_0 - \hat{h}_1 - \hat{h}_3 + \hat{h}_4 - 2(\hat{h}_7 + \hat{h}_8)] + S_3, \tag{27d}$$

$$\overline{g}_4^p = \overline{g}_4 + [\hat{h}_0 - \hat{h}_2 - \hat{h}_3 - \hat{h}_4 - 2(\hat{h}_6 + \hat{h}_8)] + S_4, \tag{27e}$$

$$\overline{g}_5^p = \overline{g}_5 + [\hat{h}_0 + \hat{h}_1 + \hat{h}_2 + 2\hat{h}_3 + \hat{h}_5 - \hat{h}_6 - \hat{h}_7 + \hat{h}_8] + S_5, \tag{27f}$$

$$\overline{g}_6^p = \overline{g}_6 + [\hat{h}_0 - \hat{h}_1 + \hat{h}_2 + 2\hat{h}_3 - \hat{h}_5 - \hat{h}_6 + \hat{h}_7 + \hat{h}_8] + S_6, \tag{27g}$$

$$\overline{g}_7^p = \overline{g}_7 + [\hat{h}_0 - \hat{h}_1 - \hat{h}_2 + 2\hat{h}_3 + \hat{h}_5 + \hat{h}_6 + \hat{h}_7 + \hat{h}_8] + S_7, \tag{27h}$$

$$\overline{g}_8^p = \overline{g}_8 + [\hat{h}_0 + \hat{h}_1 - \hat{h}_2 + 2\hat{h}_3 - \hat{h}_5 + \hat{h}_6 - \hat{h}_7 + \hat{h}_8] + S_8. \tag{27i}$$

Finally, based on the solution of the thermal cascaded LBE given in Eqs. (26a) and (26b), the temperature field T can be obtained as

$$T = \sum_\alpha g_\alpha = \sum_\alpha \overline{g}_\alpha + \frac{\delta t}{2} G. \tag{28}$$

3. Numerical results

In this section, numerical simulations of some illustrative benchmark problems are conducted to validate the accuracy of our proposed cascaded LBE model for thermal convective flows. The test problems without source terms in the energy equation are thermal Poiseuille flow, thermal flow in a channel with wall injection, and natural convection in a square cavity. Also, problems considered with variable source terms in the energy equation are a reaction-diffusion problem, and Couette flow with temperature gradients (i.e. thermal Couette flow with viscous heat dissipation). In this study, the halfway bounce-back scheme is employed to treat velocity boundary conditions while the general anti-bounce-back scheme (Zhang et al., 2012) is adopted to deal with temperature boundary conditions. In problems involving LBM solution of fuid flow all relaxation parameters are set to 1.0 except ω_4 and ω_5 (the relaxation rates for the first order moments) which are both equal to τ_f^{-1}. In the thermal model all relaxation parameters are set to 1.0 except λ_1 and λ_2 which are both equal to τ_g^{-1}.

3.1. Unsteady reaction–diffusion problem: variable source term

The unsteady reaction diffusion problem is a good problem to test the accuracy of the present LBE cascaded model for the equivalent energy equation with a variable source term. Such a system defined in the region $0 \le x,\ y \le l$, with the macroscopic governing equation written as (Meng and Guo, 2015):

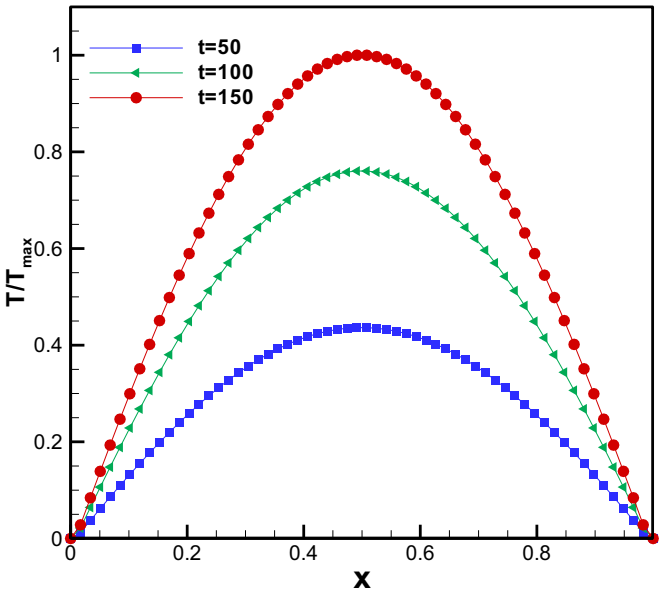

Fig. 1. Temperature profiles for the unsteady reaction-diffusion problem with a variable source term at and diffusion coefficient $\alpha = 10^{-3}$ at different times. Markers represent the Cascaded LBE results and lines represent the analytical solution.

$$\frac{\partial T}{\partial t} = \alpha\nabla^2 T + 2C\sin(\pi x/l)\sin(\pi y/l) \tag{29}$$

where $G(x, y) = 2C\sin(\pi x/l)\sin(\pi y/l)$ is the spatially varying source term, l is the width of the region, C is a constant, and α is the diffusion coefficient. The initial and boundary conditions of this system are: $T(x, y, 0) = 0$, $T(0, y, t) = T(l, y, t) = 0$, $T(x, 0, t) = T(x, l, t) = 0$.

The analytical solution of this problem is given by

$$T(x, y, t) = \frac{l^2}{\pi^2\alpha} C\left[1 - \exp\left(-\frac{2\pi^2\alpha t}{l^2}\right)\right]\sin(\pi x/l)\sin(\pi y/l), \tag{30}$$

We conduct our numerical simulation with a grid resolution of 61×61, $C = 10$ and with the thermal diffusivity coefficients $\alpha = 10^{-3}$ and $\alpha = 10^{-4}$. The simulation results and the analytical solutions are compared at three different times $t = 50$, $t = 100$, and $t = 150$ as used in Meng and Guo (2015). The relaxation time is set to $\tau_g = 0.503$. Figs. 1 and 2 show the temperature profiles for the above two values of diffusivity coefficients showing very good agreement with the analytical solutions. We also examine the spatial accuracy of the present model. In this regard, a set of simulations are performed at four different grid resolutions, i.e., 25×25, 51×51, 101×101, and 201×201 for both values of the diffusion coefficient, i.e. $\alpha = 10^{-3}$, and $\alpha = 10^{-4}$. The global relative error of temperature (E_T) used to measure the accuracy of the model is calculated as

$$E_T = \frac{\|(T_c - T_a)\|_2}{\|T_a\|_2} \tag{31}$$

where $||.||_2$ is the Euclidean norm, i.e. $\|(T_c - T_a)\|_2 = \sqrt{\sum_i (T_{c,i} - T_{a,i})^2}$, $\|(T_a)\|_2 = \sqrt{\sum_i (T_{a,i})^2}$, and T_c and T_a are the computed and the analytical solutions respectively. The relative global error of temperature for each value of diffusivity coefficient are plotted in Fig. 3. It can be seen that the global error for temperature decreases with increase in grid resolution with a slope of -2 in the log-log plot. Hence, our present cascaded LBM model for the CDE with source term is second order accurate.

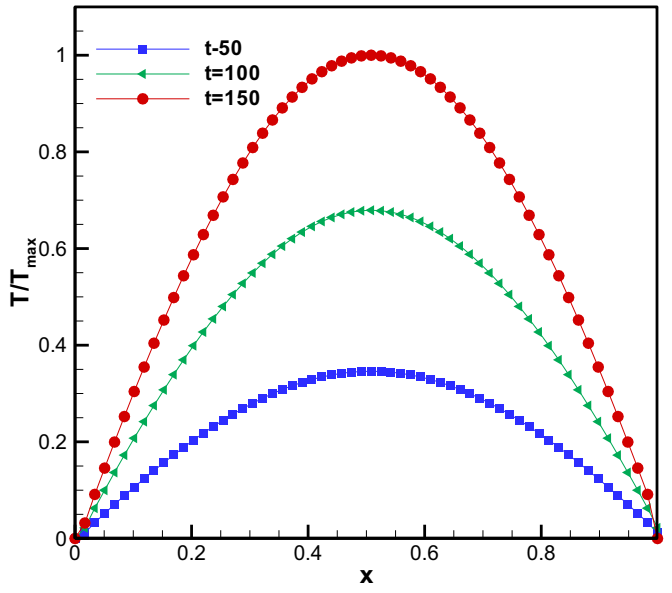

Fig. 2. Temperature profiles for the unsteady reaction-diffusion problem with a variable source term at and diffusion coefficient $\alpha = 10^{-4}$ at different times. Markers represent the Cascaded LBE results and lines represent the analytical solutions.

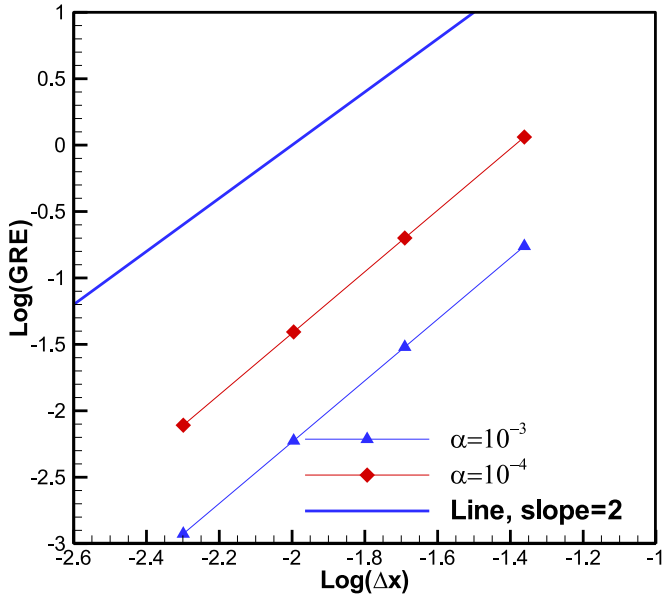

Fig. 3. Temperature global relative error at different values of the diffusion coefficient $\alpha = 10^{-3}$, $D = 0.397$, and $\alpha = 10^{-4}$, $D = 0.3997$ for the unsteady reaction-diffusion problem with variable source term.

3.2. Thermal Couette flow in a channel with wall injection

In this section, the present cascaded LBE model for thermal convective flow is employed to simulate the fully developed thermal flow in a channel, where the upper plate moves along the x-direction with velocity U_p, and a fluid is injected in the positive y-direction with a constant velocity v_0 through the stationary bottom wall. The upper wall is maintained at a higher temperature (T_h) and the bottom wall is fixed at a lower temperature (T_c). The computational domain of the problem is $0 \le x, y \le L$. In the steady state case, the analytical solutions for both velocity and temperature fields are, respectively, given by.

$$u_x(y) = \frac{\exp(Re.\ y/L) - 1}{\exp(Re) - 1}, \tag{32}$$

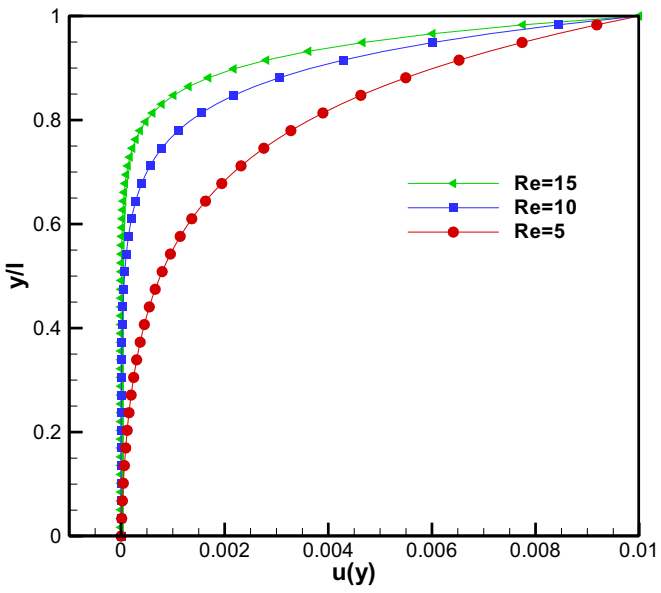

Fig. 4. Velocity profiles for thermal Couette flow in a channel with wall injection at Reynolds numbers: $Re = 5, 10, 15$. Markers represent the Cascaded LBE results and lines represent the analytical solutions.

$$T = T_c + \triangle T \frac{\exp(PrRe.\ y/L) - 1}{exp(PrRe) - 1} \tag{33}$$

where Re is the Reynolds number defined by $Re = v_0 L/\nu$, L is the width of the channel and $\triangle T$ is the temperature difference. In our numerical test, we set $U_p = v_0 = 0.01$, $T_h = 1$, $T_c = 0$, $Pr = 0.71$, with a grid size 31×61 at three different Reynolds numbers, $Re = 5$, 10, and 15.

The relaxation rates for the flow and thermal equation cascaded LB solvers are obtained based on the value of Pr and Re for each case where $\nu = Lv_0/Re$, and $\alpha = \nu/Pr$. Periodic boundary conditions are imposed at the inlet and outlet of the channel. The profiles of velocity and temperature along the y-direction at different Reynolds numbers and $Pr = 0.71$ are plotted in Figs. 4 and 5, respectively.

It is found that the numerical results agree well with the analytical solutions for this test case. We also study the grid convergence rate by

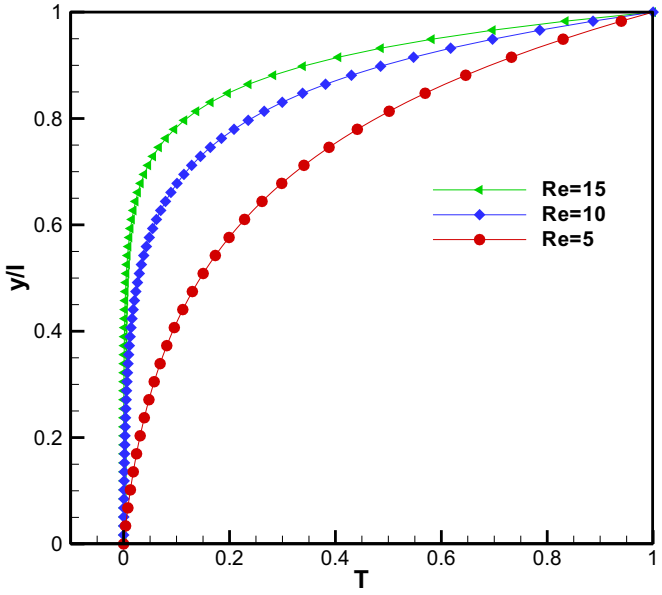

Fig. 5. Temperature profiles for thermal Couette flow in a channel with wall injection at Reynolds numbers: $Re = 5, 10, 15$. Markers represent the Cascaded LBE results and lines represent the analytical solutions.

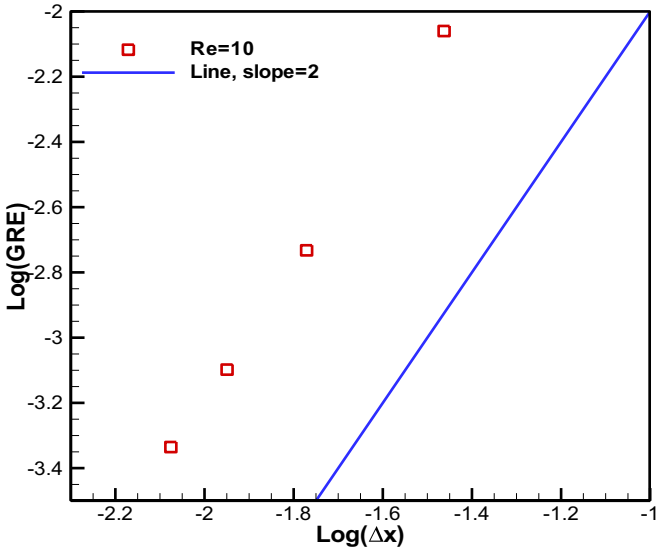

Fig. 6. Velocity relative global error of thermal Couette flow with wall injection at $Re = 10$.

considering the following grid resolutions in the y-direction $Ny = 31$, 61, 91, and 121. In these simulations, we conduct the convergence study at Reynolds numbers $Re = 5$, 10, and 15 for the above set of grid resolutions with corresponding values of the tunable parameter D as 0.05, 0.1, and 0.15, respectively. The relaxation rates are $\tau_f = \tau_g = 0.8$.

The relative global errors of velocity and temperature are plotted in Figs. 6 and 7, respectively. It can be seen that the relative errors have slopes nearly equal to − 2, which again confirms that the present cascaded LBM model for thermal flow is second order accurate. In the above, the relative global error of temperature and velocity are defined, respectively, by

$$E_T = \frac{\|(T_c - T_a)\|_2}{\|T_a\|_2} \tag{34}$$

$$E_u = \frac{\|(u_c - u_a)\|_2}{\|u_a\|_2} \tag{35}$$

where $||.||_2$ is the Euclidean norm, $\|(T_c - T_a)\|_2 = \sqrt{\sum_i (T_{c,i} - T_{a,i})^2}$, $\|(u_c - u_a)\|_2 = \sqrt{\sum_i (u_{c,i} - u_{a,i})^2}$, $\|(T_a)\|_2 = \sqrt{\sum_i (T_{a,i})^2}$, $\|(u_a)\|_2 = \sqrt{\sum_i (u_{a,i})^2}$. Here, T_c, u_c and T_a, u_a are the computed and the analytical solutions, respectively.

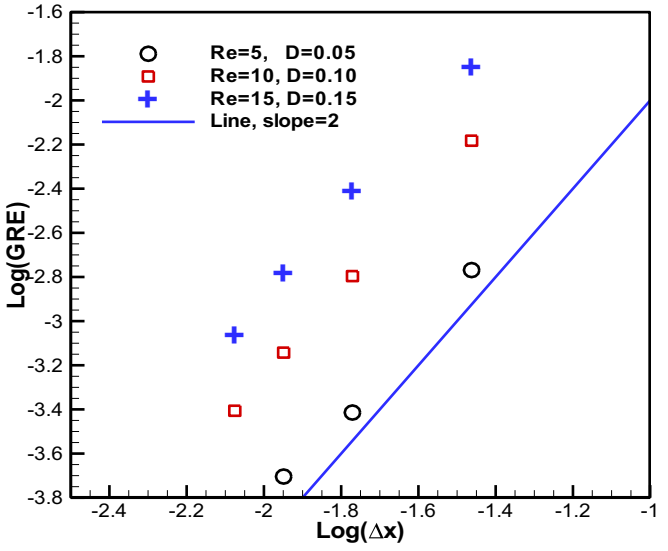

Fig. 7. Temperature relative global error of thermal Couette flow with wall injection at Reynolds numbers: $Re = 5$, 10, 15.

3.3. Diffusion in 2D Poiseuille flow

Next, we consider a 2D Poiseuille flow between two parallel plates in the streamwise direction driven by a constant body force F_x. Both the upper and bottom walls are stationary and subjected to higher (T_h) and lower (T_c) uniform temperature respectively. The computational domain is $0 \le x,\ y \le L$. Where L is the channel width. A periodic boundary condition is applied at the entrance and the exit for both velocity and temperature fields, while the halfway bounce back scheme is implemented at the solid boundaries (upper and bottom walls) for the velocity field to represent the no-slip boundary condition. The general bounce-back scheme (Zhang et al., 2012) is employed to the solid boundaries for the temperature Dirichlet boundary conditions. The analytical solution for the velocity in Poiseuille flow (parabolic profile) is given by

$$u(y) = u_{max}(1 - (y/L_H)^2), \tag{36}$$

where $u_{max} = F_x L_H^2/2\nu$ is the maximum velocity occurring halfway between the plates, ν is the kinematic viscosity related the to relaxation time τ. Here, L_H is the half distance between the two parallel plates. The analytical solution for the temperature in Poiseuille flow is given by

$$T = T_c + \triangle T(y/L), \tag{37}$$

where $\triangle T = T_h - T_c$ is the temperature difference. In our simulation, a grid size of 30 × 60 is employed. We consider two cases corresponding to different sets of Reynolds numbers $Re = u_{max}L/\nu$, Peclet numbers $Pe = u_{max}L/\alpha$ and Prandtl number $Pr = \nu/\alpha$. In the first case, we set $Pr = 0.71$, $Re = 10$ and $Pe = 7$. In the second case, we consider $Re = Pe = 10$, i.e. $Pr = 1$. Where, we consider $T_h = 1.1$, $T_c = 1$, and $\tau_f = \tau_g = 0.674$ in both cases. Fig. 8 presents a comparison of the velocity and temperature profiles for these cases. Excellent agreement with the analytical solution is exhibited in the figures.

3.4. Natural convection in a square cavity

We now present a validation study involving coupled thermal convective flow. In this regard, our cascaded LBE model is employed to simulate natural convection in a square cavity. Here, the flow is driven by the buoyancy force due to the local temperature difference against a reference temperature in the presence of gravity. The left wall is maintained at higher temperature T_h and the right wall at lower temperature T_c, while the top and bottom walls are considered to be adiabatic.The macroscopic governing equations are the convection–diffusion equation (Eq. (1)) , and the Navier–Stokes equations (Eq. (2a) and Eq. (2b)) where $\boldsymbol{F}$ is the body force which is based on the Boussinesq approximation and is given by

$$\boldsymbol{F} = g\beta(T - T_0)\hat{\boldsymbol{j}}\ . \tag{38}$$

Here, β is the thermal expansion coefficient, g is the acceleration due to gravity, $T_0 = (T_h + T_c)/2$ is the reference temperature, $\hat{\boldsymbol{j}}$ is the unit vector in the positive y-direction. This classical natural convection problem is governed by two non-dimensional parameters: The Prandtl number Pr and the Rayleigh number Ra, which are given by

$$Pr = \frac{\nu}{\alpha}, \tag{39}$$

$$Ra = \frac{g\beta\triangle TH^3}{\nu\alpha}, \tag{40}$$

where $\triangle T = T_h - T_c$ is the temperature difference between hot and cold walls, and H is the height of the square cavity.

The boundary conditions on the cavity walls can then be

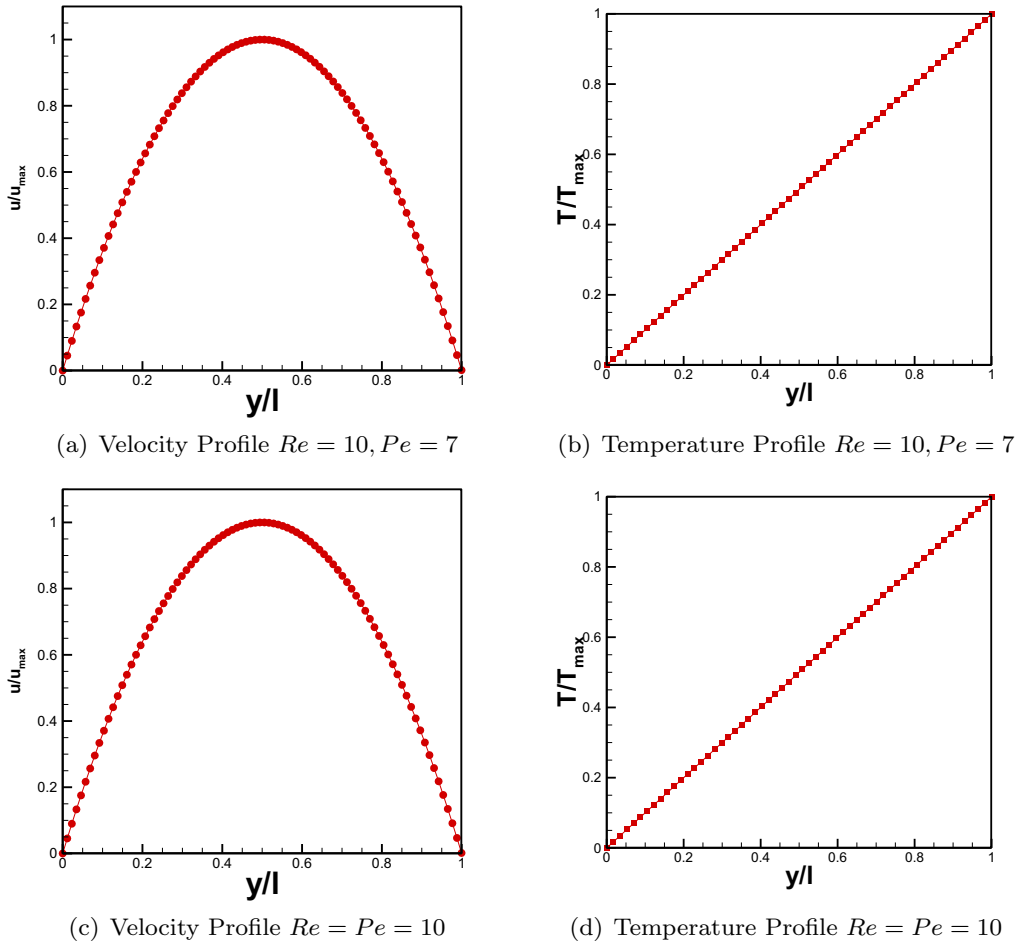

(a) Velocity Profile $Re = 10, Pe = 7$ (b) Temperature Profile $Re = 10, Pe = 7$

(c) Velocity Profile $Re = Pe = 10$ (d) Temperature Profile $Re = Pe = 10$

Fig. 8. Velocity and temperature profiles of Poiseuille flow with thermal diffusion at different values of *Re* and *Pe*. Markers represent the Cascaded LBE results and lines represent the analytical solution.

summarized as:

On the left wall:

$$u_x = u_y = 0, \qquad T = T_h = 21, \tag{41}$$

On the right wall:

$$u_x = u_y = 0, \qquad T = T_c = 1, \tag{42}$$

On the top wall:

$$u_x = u_y = 0, \qquad \frac{\partial T}{\partial y} = 0, \tag{43}$$

On the bottom wall:

$$u_x = u_y = 0, \qquad \frac{\partial T}{\partial y} = 0. \tag{44}$$

In these simulations, $Pr = 0.71$, the relaxation times for fluid flow and temperature are set as $\tau_f = 0.55$ and $\tau_g = 0.57$, respectively. The streamlines and the isotherms for the ranges of Rayleigh number *Ra* between 10^3 and 10^6 are shown in Fig. 11. Also, the vorticity contours for $Ra = 10^3 - 10^6$ are shown in Fig. 12. The streamlines, isotherms and vorticity contours are in very good correspondence and consistent with prior benchmark solution results (de Vahl Davis, 1983; Hortmann et al., 1990). The natural convection flow patterns become more complex as *Ra* increases. In order to characterize this in more detail, the temperature at the vertical and horizontal mid-planes of the square cavity, i.e. $x/H = 0.5$ and $y/H = 0.5$, respectively, for various Rayleigh numbers ($Ra = 10^3 - 10^6$) are presented in Figs. 9 and 10. From Figs. 9 and 10, it is seen that the temperature contour lines become almost horizontal around the center of the cavity as the Rayleigh number *Ra*

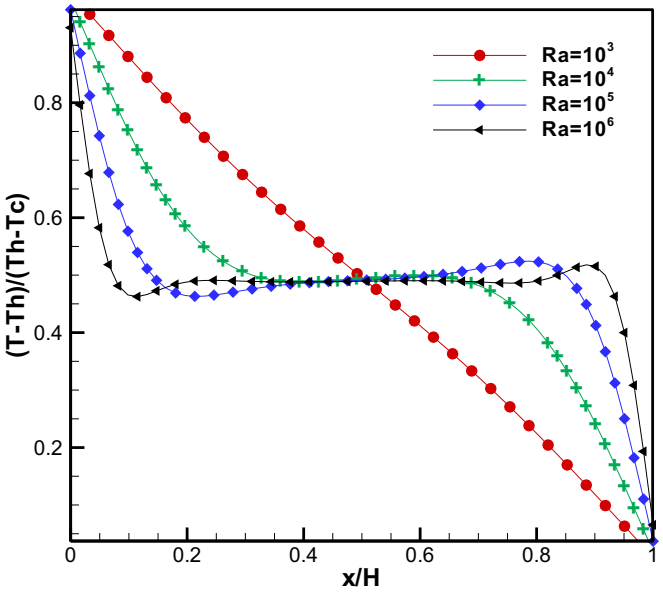

Fig. 9. Temperature profiles along horizontal centerline of the cavity at various Rayleigh numbers: $Ra = 10^3$, 10^4, 10^5, and 10^6 computed using the cascaded LBM.

increases. The streamlines become more packed next to the side wall as *Ra* increases, i.e. the fluid moves faster as natural convection is intensified. In these cases, the value of the factor $g\beta$ needed in the simulation is obtained as a function of Rayleigh number *Ra* using

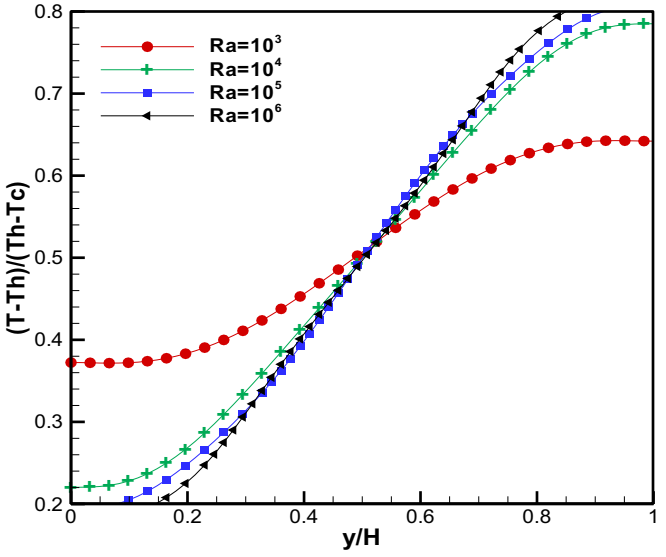

Fig. 10. Temperature profiles along the vertical centerline of the cavity flow at various Rayleigh numbers $Ra = 10^3$, 10^4, 10^5, and 10^6 computed using the cascaded LBM.

$$g\beta = \frac{\nu\alpha Ra}{\triangle TH^3}. \tag{45}$$

The representative values of $g\beta$ corresponding to each Ra is shown in Table 1.

Finally, Table 2 shows quantitative comparison between the key parameters for this problem (average Nusselt number, maximum velocity magnitudes and their locations) between the present cascaded LBE results and benchmark data (de Vahl Davis, 1983; Hortmann et al., 1990). Excellent agreement is seen (within 0.01%). The streamlines and isotherms for all Rayleigh numbers $Ra = (10^3 - 10^6)$ as shown in Fig. 11 indicate that the computed results using the present cascaded LBM are in excellent agreement with results given by de Vahl Davis (1983) and Hortmann et al. (1990).

3.5. Thermal Couette flow with viscous heat dissipation: modeling a heat source

Finally, we consider the simulation of Couette flow with temperature gradient to test the ability of the present thermal cascaded LB model with a source term to describe the viscous heat dissipation. We consider 2D thermal Couette flow between two parallel plates, where the upper plate moves along x-direction with a velocity U, and at higher temperature T_h, whereas the bottom wall is stationary and maintained at lower temperature T_c; L is the distance between the two plates. In this case, the source term G in the thermal energy equation, Eq. (1) is the viscous heat dissipation given by

$$G = \frac{2\nu}{C_p}(\boldsymbol{S}\colon \boldsymbol{S}), \tag{46}$$

$$\boldsymbol{S} = \frac{1}{2}(\nabla\boldsymbol{u} + (\nabla\boldsymbol{u})^T), \tag{47}$$

where $\boldsymbol{S}$ is strain rate tensor, and C_p is the specific heat at constant pressure. The macroscopic governing equations for momentum and energy can be written, respectively, as:

$$\frac{\partial^2 u}{\partial y^2} = 0, \tag{48}$$

$$\alpha\frac{\partial^2 T}{\partial y^2} + \frac{\nu}{C_p}\left[\frac{\partial u}{\partial y}\right]^2 = 0. \tag{49}$$

The analytical solutions for the velocity and temperature are then given by:

$$u(y) = U\frac{y}{L}, \qquad v = 0, \tag{50}$$

$$\frac{T - T_c}{T_h - T_c} = \frac{y}{L} + 0.5Br\frac{y}{L}\left(1 - \frac{y}{L}\right), \tag{51}$$

where $Ec = \frac{U^2}{Cp(T_h - T_c)}$ is the Eckert number, and $Pr = \nu/\alpha$ is the Prandtl number, and the effect of viscous heat dissipation is controlled by the Brinkman number $Br = EcPr$. In this simulation, we set the relaxation time $\tau_f = 0.9$, and the lower temperature $T_c = 1$ with a grid resolution of 5×41, $Re = 10$, and $Pr = 0.71$ at Eckert numbers 7, 14, and 28. For the solution of this problem, it is important to note that the convection diffusion equation with a source term (1) is coupled with Navier–Stokes (N–S) Eqs. (2a) and (2b). The cascaded LB fluid model (Geier et al., 2006) is used to solve the N–S equations. The source term G in Eq. (46) can be written as

$$G = \frac{2\nu}{cp}[S_{xx}^2 + S_{yy}^2 + 2S_{xy}^2]. \tag{52}$$

In this case, we have

$$S_{xx} = \frac{\partial u}{\partial x} = 0, \quad S_{yy} = \frac{\partial v}{\partial y} = 0, \quad S_{xy} = \frac{1}{2}\left(\frac{\partial u}{\partial y} + \frac{\partial v}{\partial x}\right). \tag{53}$$

These strain rate components can be computed locally using the non-equilibrium moments in the cascaded LBE for the fluid flow as mentioned in Premnath and Banerjee (2009). Fig. 13 shows the temperature profiles for different Eckert numbers. In addition, we carried out simulations for different values of Prandtl numbers, 0.25, 1.25, and 2.5 with the Eckert number being fixed at 8 with a grid size 5×41. Fig. 14 shows the temperature profiles for different Prandtl numbers. In both these cases, very good agreement between the cascaded LBM results and analytical solutions are exhibited. Next, we study the grid convergence rate for the case with a fixed $Ec = 8$ at different values of the Prandtl number: 0.25, 1.25, and 2.5.Here, we set $U = 0.07$, $\tau_g = 0.9$. The values of the tunable parameter D at these Prandtl numbers are -1.2, 0.08, and 0.24, respectively. We also conduct a grid convergence study for the case where the Prandtl number is fixed at $Pr = 0.71$ while the Eckert number is changed as 7, 14 and 28, $\tau_g = 1.0638$, and $D = 0$. Three grid resolutions in the y-direction ($N_y = 41, 81$, and 161) are employed in the convergence study. Figs. 15 and 16 show that the slope of the temperature relative global error is about -2, i.e. the present thermal cascaded LB model is of second order accuracy in space.

Couette flow with viscous heat dissipation was also used to test the ability of the present thermal cascaded lattice Boltzmann model to simulate relatively high Peclet numbers at a low grid resolution of 5×23. The analytical solution for temperature is given by Eq. (51), Here, the Brinkman number Br is rewritten as $Br = \frac{PeEc}{Re}$

$$\frac{T - T_c}{T_h - T_c} = \frac{y}{L}\left[1 + 0.5\left(\frac{PeEc}{Re}\right)\left(1 - \frac{y}{L}\right)\right], \tag{54}$$

where Pe is the Peclet number. In this case study, the temperature profiles for a fixed Reynolds number ($Re = 10$), and Eckert number ($Ec = 0.1$) at different values of Peclet numbers 10, 10^2, 10^3, 10^4, 10^5 and 10^6 (corresponding to Brinkman numbers $Br = 10^{-1}$, 1, 10^1, 10^2, 10^3 and 10^4) are shown in Fig. 17. Here, we set $T_h = 1$, $T_c = 0$, and $\tau_g = 0.94$. The values of the tunable parameter D corresponding to the above Peclet numbers are 0, 0.3970,0.4366,0.4406,0.4409, and 0.4410,

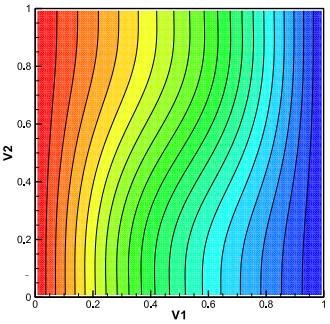

(a) Isotherms $Ra = 10^3$

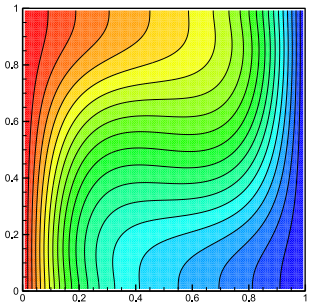

(b) Isotherms $Ra = 10^4$

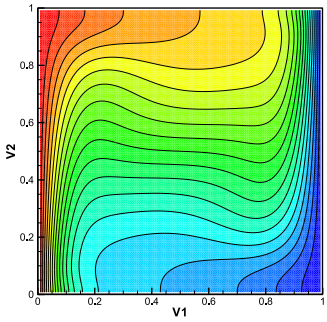

(c) Isotherms $Ra = 10^5$

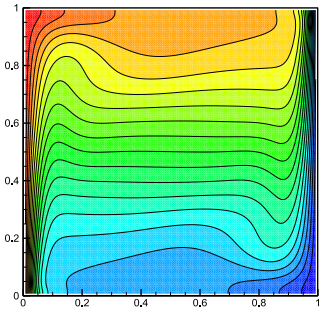

(d) Isotherms $Ra = 10^6$

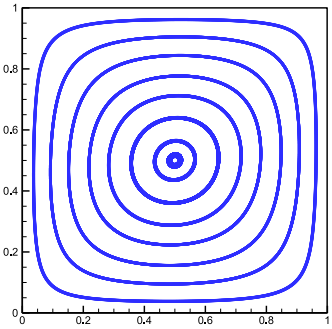

(e) Streamlines $Ra = 10^3$

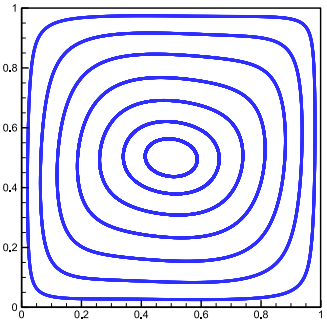

(f) Streamlines $Ra = 10^4$

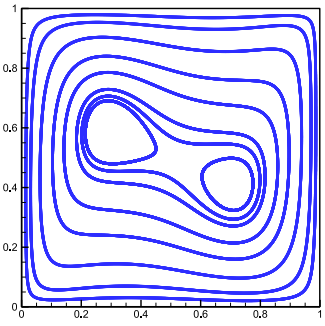

(g) Streamlines $Ra = 10^5$

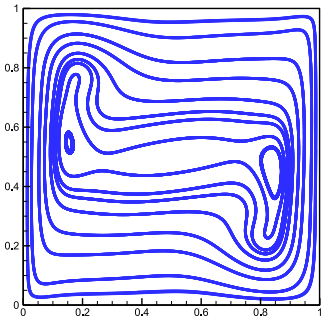

(h) Streamlines $Ra = 10^6$

Fig. 11. Isotherms and streamlines at different values of Rayleigh numbers $Ra = 10^3$, 10^4, 10^5 and 10^6 for natural convection in a square cavity computed using the cascaded LBM.

respectively. Excellent agreement between the cascaded LBM results and the analytical solution is seen for relatively high Peclet numbers. This result is indicative of the improved stability properties of the cascaded LBM as researchers utilizing SRT LBM (Shi et al., 2004) only presented results for Brinkman numbers up to $Br = 100$. A convergence study was done for this problem at different values of Peclet numbers 10, 10^2, and 10^3 for grid resolutions $N_y = 81,161$, and 321, $\tau_g = 0.9$, and tunable parameters D at each Peclet number is set to be 0, 0.36, and 0.696, respectively. The relative global error of temperature against the various grid resolutions is shown in Fig. 18. It is evident that the slope

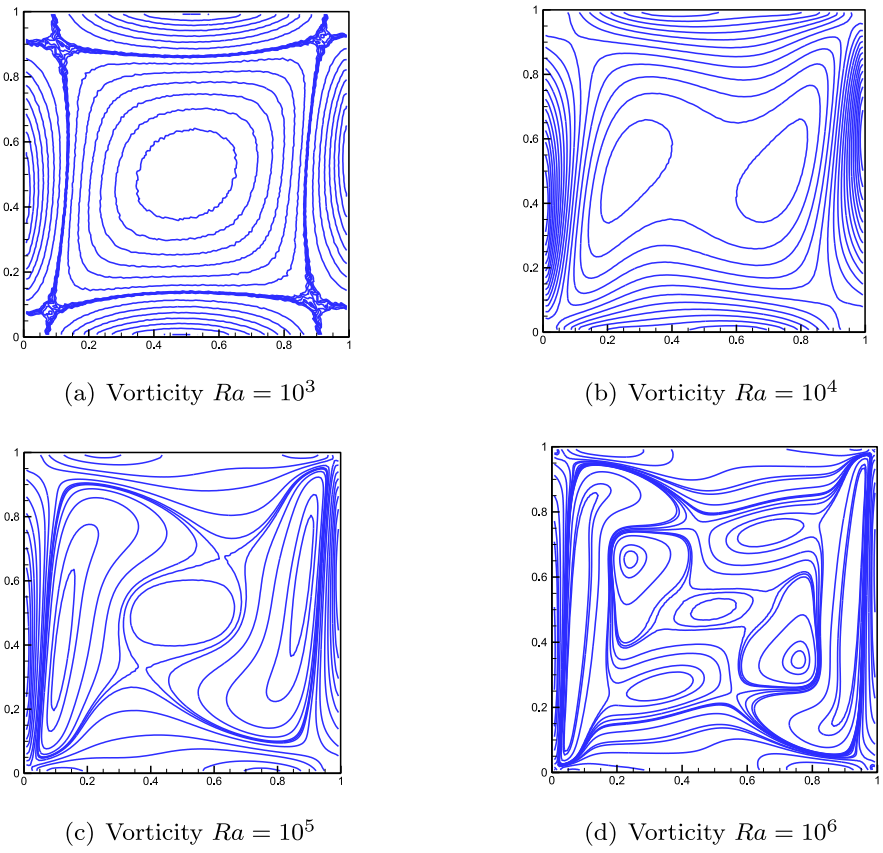

(a) Vorticity $Ra = 10^3$ (b) Vorticity $Ra = 10^4$

(c) Vorticity $Ra = 10^5$ (d) Vorticity $Ra = 10^6$

Fig. 12. Vorticity contours at various Rayleigh numbers $Ra = 10^3$, 10^4, 10^5 and 10^6 for natural convection in a square cavity computed using the LBM.

Table 1
Values of $g\beta$ corresponding to each Rayleigh number used in the simulation of natural convection in a square cavity.

Rayleigh number Ra	Grid size ($N_x \times N_y$)	$g\beta = \frac{Ra.\nu.\alpha}{\Delta T H^3}$
10^3	128×128	9.44×10^{-9}
10^4	128×128	9.44×10^{-8}
10^5	128×128	9.44×10^{-7}
10^6	128×128	9.44×10^{-6}

of the temperature relative global error is near -2, i.e. the present thermal cascaded LB model is second order in space at relatively high Peclet numbers.

3.6. Convection–diffusion of a Gaussian hill: stability test

Finally, we consider the convection diffusion equation (Eq. (1)) where $\mathbf{u} = u_o\hat{\mathbf{i}} + v_o\hat{\mathbf{j}}$ is a prescribed 2-D uniform velocity field and subjected to the Gaussian hill initial condition

$$T(x, y, 0) = \frac{T_o}{2\pi\sigma_o^2}\exp\left(\frac{-[x^2 + y^2]}{2\sigma_o^2}\right), \tag{55}$$

where the parameter σ_o controls the width of the profile. The analytical solution of this problem is given by

$$T(x, y, t) = \frac{T_o}{2\pi(\sigma_o^2 + 2\alpha t)}\exp\left(\frac{-[(x - u_o t)^2 + (y - v_o t)^2]}{2(\sigma_o^2 + 2\alpha t)}\right). \tag{56}$$

We set $\sigma_o = 0.05$ and advect the profile with the diagonal velocity vector with components $u_o = v_o = 0.25c_s$. We choose $T_o = 2\pi\sigma_o^2$ so that the initial profile has a peak magnitude of 1.0. Periodic boundary conditions for the temperature are employed. In what follows we vary the fluid diffusivity to compare the stability characteristics of the cascaded centeral moment LBM with the SRT and MRT implementations of the LBM. We consider the MRT method in Meng and Guo (2015) and we set the tunable parameter D in both methods to be zero. In the three methods, the fluid diffusivity is given by $\alpha = {c_s}^2\left(\frac{1}{\lambda} - \frac{1}{2}\right)$ where λ is the relaxation rate of the first order moments corresponding to the equilibrium moments u_xT and u_yT in the cascaded and MRT LBM. We use a 521×521 grid and vary the diffusivity by varying the relaxation time $\tau_g = \frac{1}{\lambda}$. Comparison of the cascaded and MRT LBM methods is complicated by the large number of relaxation parameters associated with each method. We set the relaxation time for the first order moments to τ_g based on flow parameters. We then set all other relaxation times to 1.0. With this choice of parameters we are relaxing the energy fluxes (first order moments) at the same rate in both methods. This choice of parameters is not necessarily optimal for either method but it does gives us a rational basis for comparison.

The simulation is run for 1000 time increments at which time the Gaussian profile has convected from the center of the domain to the upper right corner. Temperature contours for the analytic solution and the results from a cascaded LBM simulation at the initial and final state are shown in Fig. 19. A closer view of the final profiles along with the lattice coordinates is given in Fig. 20.

Finally, we consider numerical stability results from the SRT, MRT, and cascaded LBM at various values of the relaxation time τ_g. Table 3 provides the numerical stability and global relative error (given by Eq.

Table 2
Comparison between numerical results obtained using the cascaded LBM and the published results (de Vahl Davis, 1983; Hortmann et al., 1990) at different Rayleigh numbers ($Ra = 10^3 - 10^6$).

Ra	Parameter	Present cascaded LBM	de Vahl Davis (1983)	Hortmann et al. (1990)
10^3	$\overline{Nu}$	1.117	1.116	NA
	u_{max}	3.605	3.634	NA
	y_{max}	0.816	0.813	NA
	v_{max}	3.654	3.679	NA
	x_{max}	0.176	0.179	NA
	$\|\Psi\|_{max}$	1.16	1.174	NA
10^4	$\overline{Nu}$	2.237	2.234	2.24475
	u_{max}	16.182	16.182	16.1759
	y_{max}	0.824	0.823	0.8255
	v_{max}	19.551	19.509	19.6242
	x_{max}	0.12	0.12	0.12
	$\|\Psi\|_{max}$	5.079	5.098	NA
10^5	$\overline{Nu}$	4.509	4.51	4.521
	u_{max}	35.137	34.81	34.7398
	y_{max}	0.856	0.855	0.85312
	v_{max}	68.511	68.22	68.6465
	x_{max}	0.064	0.066	0.0656
	$\|\Psi\|_{max}$	9.189	9.144	NA
10^6	$\overline{Nu}$	8.797	8.798	8.825
	u_{max}	65.57	65.33	64.8659
	y_{max}	0.856	0.851	0.85312
	v_{max}	219.95	216.75	219.861
	x_{max}	0.032	0.0387	0.0406
	$\|\Psi\|_{max}$	16.519	16.53	NA

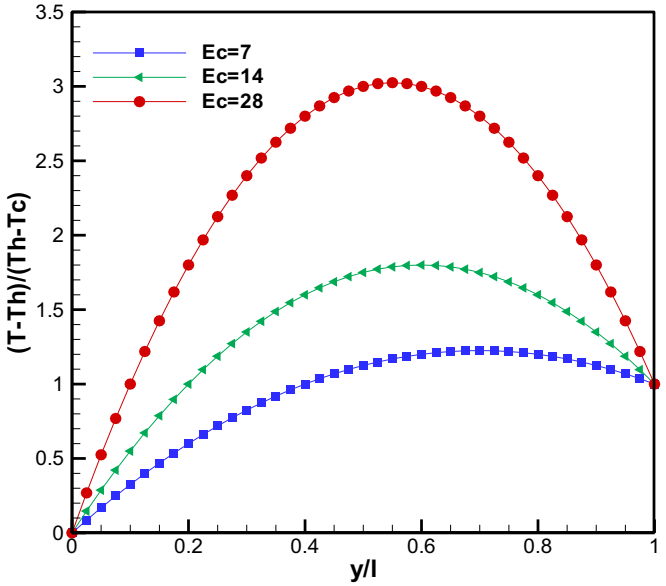

Fig. 13. Temperature profiles in Couette flow at various values of Eckert number. Markers represent the cascaded LBE simulations and lines represent the analytical solutions.

(31)) indicates the accuracy of the three methods is similar. The table also indicates that the SRT LBM is not stable at the smaller diffusivities and that the MRT is eventually not stable at the still smaller diffusivity for which the cascaded LBM is stable. It is likely that relaxation rates for the higher moments of the MRT and cascaded LB methods may be found that result in more stable behavior but this short study on the CDE concurs with other work that indicate superior stability characteristics of the cascaded LBM (Geier et al., 2015; Ning et al., 2016).

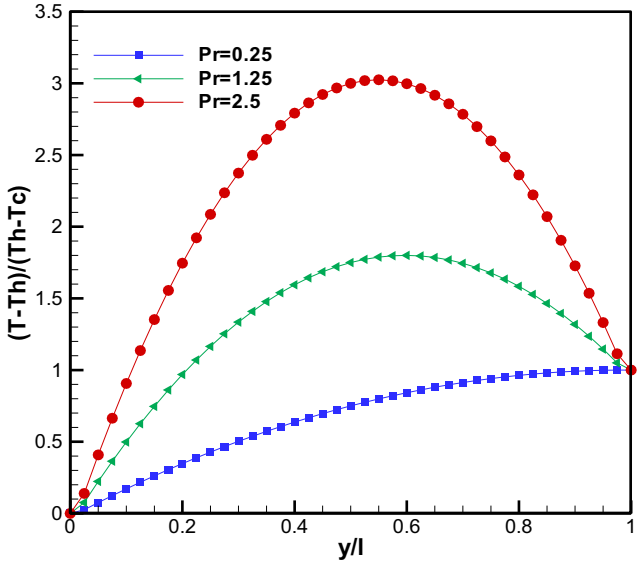

Fig. 14. Temperature profiles in Couette flow with different values of Prandtl number. Markers represent the cascaded LBE simulations and lines represent the analytical solutions.

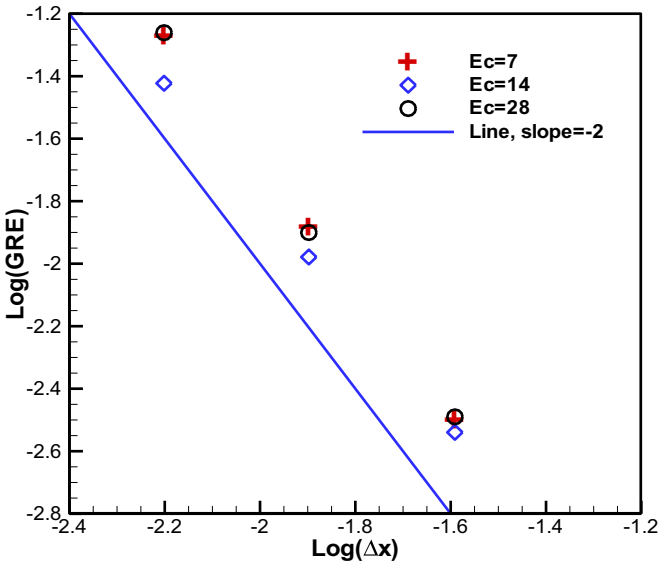

Fig. 15. Temperature global relative error at different Eckert numbers 7, 14, and 28 for thermal Couette flow with viscous heat dissipation.

4. Summary and conclusions

In this work, we presented a thermal cascaded (LB) MRT model based on central moments and including a source term. This model solves the convection–diffusion equation (CDE) for the temperature field within the double distribution function framework for the D2Q9 lattice, where the fluid motion is represented by another cascaded LB model constructed in prior work. The collision operator for the thermal field has significantly different cascaded structure for its collision kernel when compared to that for the flow field due to the differences in the number of collision invariants between them. A consistent second order scheme to incorporate the effect of locally varying heat sources by means of a variable transformation for the thermal cascaded LB model is also discussed. A Chapman–Enskog analysis of the thermal cascaded

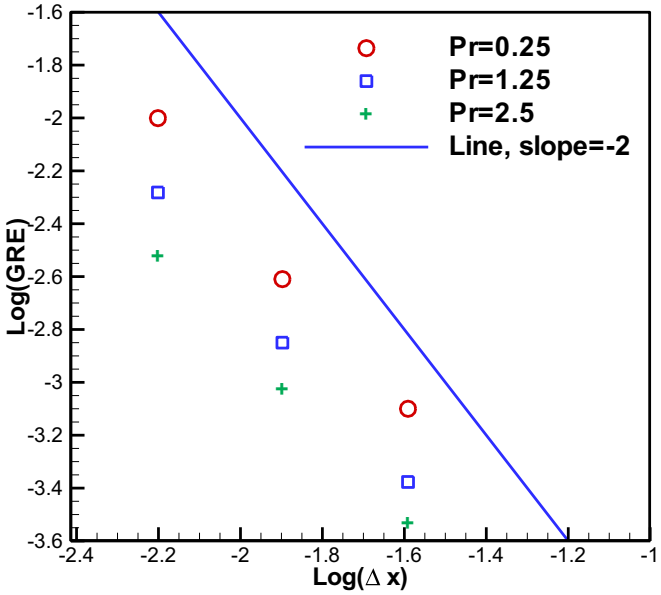

Fig. 16. Temperature global relative error at different Prandtl numbers 0.25, 1.25, and 2.5 for thermal Couette flow with viscous heat dissipation.

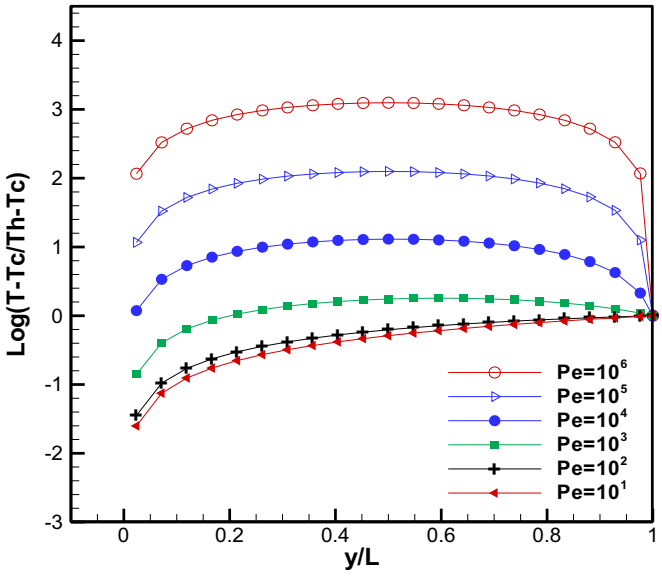

Fig. 17. Temperature profiles in thermal Couette flow at various values of Peclet numbers: Pe = 10, 10^2, 10^3, 10^4, 10^5 and 10^6. Markers represent the Cascaded LBE results and lines represent the analytical solution.

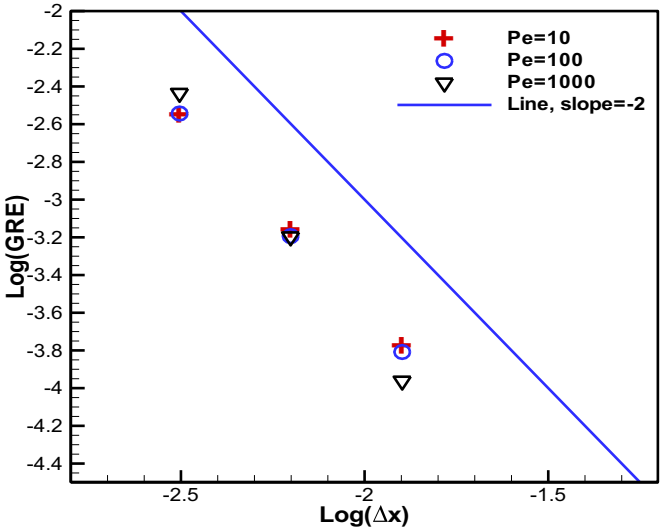

Fig. 18. Temperature global relative error at different Peclet numbers: Pe = 10, 10^2, and 10^3 for thermal Couette flow with viscous heat dissipation.

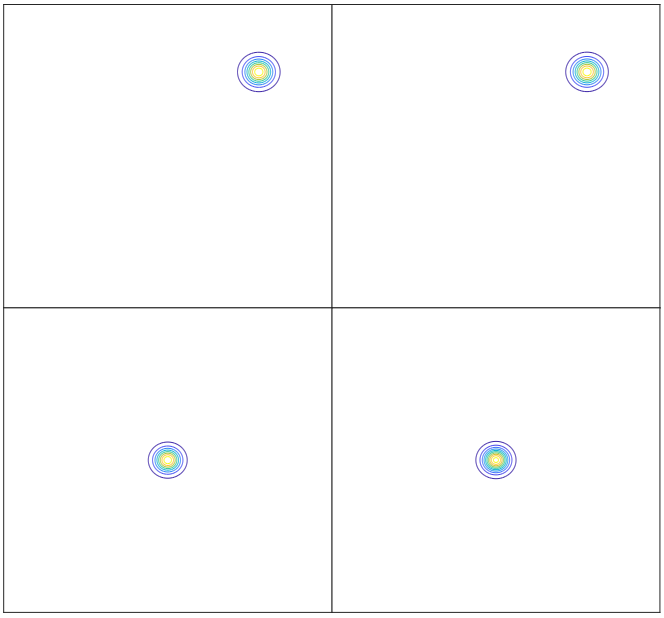

Fig. 19. Temperature contours for the convection–diffusion of a Gaussian hill problem with τ_g = 0.55. Bottom left: Analytic solution initial condition. Top left: Analytic solution after 1000 time increments. Bottom right: Cascaded LBM solution initial condition. Top right: Cascaded LBM solution after 1000 time increments. Temperature contours are from 0.05 up to 0.95 in increments of 0.05.

LB model shows its consistency with the CDE including a source term. It also provides expressions for temperature gradients in the augmented moment equilibria in terms of locally known non-equilibrium moments.

The new thermal cascaded LBE is validated for a number of benchmark problems, including thermal Poiseuille flow, thermal Couette flow and natural convection in a square cavity. Comparison of the temperature profiles under different conditions for these problems, as well as the average Nusselt number at different Rayleigh numbers in the case of the natural convection within a square cavity, with prior benchmark results demonstrate high accuracy of the thermal cascaded LBE model. Furthermore, it is shown numerically that the model is second order accurate in space for a range of thermal convective flow problems. Finally, the thermal cascaded LB model exhibits improved stability characteristics over the SRT LBM and the conventional MRT LBM. The cascaded LBM for fluid flow has been shown to improve

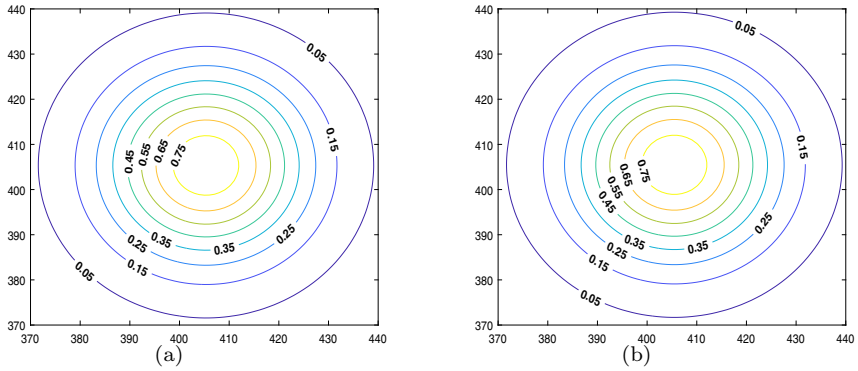

Fig. 20. Temperature contours for the convection–diffusion of a Gaussian hill problem with $\tau_g = 0.55$ after 1000 time increments.(a) Analytic solution. (b) Cascaded LBM solution.

Table 3
Global relative error and stability characteristics after 1000 time increments for SRT, MRT, and Cascaded LBM for different relaxation times for the convection–diffusion of a Gaussian hill problem at a Mach number of 0.25.

τ_g	0.55	0.51	0.501
α	1.67×10^{-2}	3.33×10^{-3}	3.33×10^{-4}
SRT	0.0097	Unstable	Unstable
MRT	0.0086	0.0096	Unstable
Cascaded	0.0101	0.0108	0.0110

stability at high Reynolds numbers typically encountered in turbulent flows (Geier et al., 2015) and the improved stability of the thermal cascaded LB MRT model should be useful for simulating turbulent flows such as the high Rayleigh number DNS simulations found in Dixit and Babu (2006). We note also that Dixit and Babu (2006) used an SRT model and hence were restricted to Prandtl numbers near 1/2, while the conventional MRT as well as the thermal cascaded LB MRT model would relieve this restriction.

Acknowledgments

The senior authors (SWJ Welch and KN Premnath) would like to acknowledge the support ot the US National Science Foundation (NSF) under Grant CBET-1705630.

Appendix A. Construction of the Cascaded Collision Operator for the Temperature Field

The collision operator for the thermal cascaded LBE can be constructed by starting from the lowest order non-conserved (i.e. first order) post-collision central moments, tentatively setting them to their equilibrium states and then multiplying the resulting expression for the collision kernel, $\widehat{h}_\beta$, by a corresponding relaxation parameter λ_β to allow for a relaxation process during collision (Geier et al., 2006). Here, only those terms that are not in the post-collision states for the lower order moments are multiplied by the relaxation parameters. Thus, we start from the first order post-collision central moment, i.e. $\langle \overline{g}_\alpha^p | (e_{\alpha x} - u_x) \rangle$ and $\langle \overline{g}_\alpha^p | (e_{\alpha y} - u_y) \rangle$ and tentatively set them equal to $\hat{\kappa}_x^{eq}$ and $\hat{\kappa}_y^{eq}$, respectively. In particular,

$$\hat{\kappa}_x^{eq} = 0 = \langle \overline{g}_\alpha^p | (e_{\alpha x} - u_x \rangle = \langle \overline{g}_\alpha^p | e_{\alpha x} \rangle - u_x \langle \overline{g}_\alpha^p | T \rangle, \tag{A.1}$$

where from Eq. (27b) raw moments of the post-collision distribution function in terms of its pre-collision value, the collision kernel, and the source term are used to obtain the right hand sides of the above equation. That is,

$$\langle \overline{g}_\alpha^p | e_{\alpha x} \rangle = \langle \overline{g}_\alpha | e_{\alpha x} \rangle + \langle (\mathscr{K} \cdot \widehat{\mathbf{h}})_\alpha | e_{\alpha x} \rangle + \langle S_\alpha | e_{\alpha x} \rangle = \hat{\overline{\kappa}}_x^{'} + 6\widehat{h}_1 + \hat{\sigma}_x^{'},$$
$$\langle \overline{g}_\alpha^p | T \rangle = \langle \overline{g}_\alpha | T \rangle + \langle (\mathscr{K} \cdot \widehat{\mathbf{h}})_\alpha | T \rangle + \langle S_\alpha | T \rangle = T + \frac{1}{2} G.$$

Substituting the above expressions in Eq. (A.1) and rearranging, and solving for the first component of the collision kernel we get the following tentative expression

$$\widehat{h}_1 = \frac{1}{6} \left\{ \hat{\kappa}_x^{'eq} - \hat{\overline{\kappa}}_x^{'} - \frac{1}{2} \hat{\sigma}_x^{'} \right\} \tag{A.2}$$

where $\hat{\kappa}_x^{'eq} = u_x T$. In order to provide further flexibility in adjusting the transport coefficient in the CDE, the raw moment equilibrium $\hat{\kappa}_x^{'eq}$ will be augmented with an extended moment equilibrium $\frac{1}{3} D \delta t \, (\partial_x T)$, where D is the adjustable parameter. See Appendix B for an analysis of such a scheme. In addition, we apply a relaxation parameter λ_1 in the equation above Eq. (A.2) to reflect the collision as a relaxation process. Thus, we get

$$\widehat{h}_1 = \frac{\lambda_1}{6} \left\{ \hat{\kappa}_x^{'eq} - \hat{\overline{\kappa}}_x^{'} - \frac{1}{2} \hat{\sigma}_x^{'} + \frac{1}{3} D \delta t \left(\partial_x T \right) \right\}. \tag{A.3}$$

Similarly, setting $\langle \overline{g}_\alpha^p | (e_{\alpha y} - u_y) \rangle$ to $\hat{\kappa}_y^{eq} = 0$ and using

$$\langle \overline{g}_\alpha^p | e_{\alpha y} \rangle = \langle \overline{g}_\alpha | e_{\alpha y} \rangle + \langle (\mathscr{K} \cdot \widehat{\mathbf{h}})_\alpha | e_{\alpha y} \rangle + \langle S_\alpha | e_{\alpha y} \rangle = \hat{\overline{\kappa}}_y^{'} + 6\widehat{h}_2 + \hat{\sigma}_y^{'},$$

and following the same procedure as above, we obtain

$$\widehat{h}_2 = \frac{\lambda_2}{6} \left\{ \hat{\kappa}_y^{'eq} - \hat{\overline{\kappa}}_y^{'} - \frac{1}{2} \hat{\sigma}_y^{'} + \frac{1}{3} D \delta t \left(\partial_y T \right) \right\}. \tag{A.4}$$

Here, $\hat{\kappa}_y^{'eq} = u_y T$. In the above, the temperature gradient needed in the extended moment equilibria can be locally computed in terms of the first order non-equilibrium moments (see Appendix B for details). Next, consider the second order diagonal central moments and tentatively set them to their corresponding equilibrium states, i.e.

$$\hat{\kappa}_{xx}^{eq} = c_s^2 T = \langle \overline{g}_\alpha^p | (e_{\alpha x} - u_x)^2 \rangle = \langle \overline{g}_\alpha^p | (e_{\alpha x}^2 \rangle - 2u_x \langle \overline{g}_\alpha^p | e_{\alpha x} \rangle + u_x^2 \langle \overline{g}_\alpha^p | T \rangle. \tag{A.5}$$

and

$$\hat{\kappa}_{yy}^{eq} = c_s^2 T = \langle \overline{g}_\alpha^p | (e_{\alpha y} - u_y)^2 \rangle = \langle \overline{g}_\alpha^p | (e_{\alpha y}^2 \rangle - 2u_y \langle \overline{g}_\alpha^p | e_{\alpha y} \rangle + u_y^2 \langle \overline{g}_\alpha^p | T \rangle. \tag{A.6}$$

Then, using

$$\langle \overline{g}_\alpha^p | e_{\alpha x}^2 \rangle = \langle \overline{g}_\alpha | e_{\alpha x}^2 \rangle + \langle (\mathscr{K} \cdot \hat{\mathbf{h}})_\alpha | e_{\alpha x}^2 \rangle + \langle S_\alpha | e_{\alpha x}^2 \rangle = \hat{\bar{\kappa}}_{xx}^{'} + 6\hat{h}_3 + 2\hat{h}_4 + \hat{\sigma}_{xx}^{'}$$

$$\langle \overline{g}_\alpha^p | e_{\alpha y}^2 \rangle = \langle \overline{g}_\alpha | e_{\alpha y}^2 \rangle + \langle (\mathscr{K} \cdot \hat{\mathbf{h}})_\alpha | e_{\alpha y}^2 \rangle + \langle S_\alpha | e_{\alpha y}^2 \rangle = \hat{\bar{\kappa}}_{yy}^{'} + 6\hat{h}_3 - 2\hat{h}_4 + \hat{\sigma}_{yy}^{'}$$

and substituting the above two expressions in Eqs. (A.5) and (A.6), respectively, and rearranging we get

$$6\hat{h}_3 + 2\hat{h}_4 = \frac{1}{3}T - u_x^2 T - \hat{\bar{\kappa}}_{xx}^{'} + 2u_x \hat{\bar{\kappa}}_x^{'} - \hat{\sigma}_{xx}^{'} + 2u_x \hat{\sigma}_x^{'} - \frac{1}{2}u_x^2 G + 12u_x \hat{h}_1. \tag{A.7}$$

$$6\hat{h}_3 - 2\hat{h}_4 = \frac{1}{3}T - u_y^2 T - \hat{\bar{\kappa}}_{yy}^{'} + 2u_y \hat{\bar{\kappa}}_y^{'} - \hat{\sigma}_{yy}^{'} + 2u_y \hat{\sigma}_y^{'} - \frac{1}{2}u_y^2 G + 12u_y \hat{h}_2. \tag{A.8}$$

Solving for $\hat{h}_3$ and $\hat{h}_4$ from the above two equations and then applying the relaxation parameters λ_3 and λ_4, respectively, for $\hat{h}_3$ and $\hat{h}_4$, while excluding the lower order collision kernel terms (i.e. $\hat{h}_1$ and $\hat{h}_2$) as they are already in the post-collision state, we finally get

$$\begin{aligned} \hat{h}_3 &= \frac{\lambda_3}{12}\left\{\frac{2}{3}T - (u_x^2 + u_y^2)T - \left(\hat{\bar{\kappa}}_{xx}^{'} + \hat{\bar{\kappa}}_{yy}^{'}\right) + 2u_x \hat{\bar{\kappa}}_x^{'} + 2u_y \hat{\bar{\kappa}}_y^{'} \right. \\ &\quad \left. + \frac{1}{2}(\hat{\sigma}_{xx}^{'} + \hat{\sigma}_{yy}^{'})\right\} + u_x \hat{h}_1 + u_y \hat{h}_2, \end{aligned} \tag{A.9}$$

$$\hat{h}_4 = \frac{\lambda_4}{4}\left\{-(u_x^2 - u_y^2)T - \left(\hat{\bar{\kappa}}_{xx}^{'} - \hat{\bar{\kappa}}_{yy}^{'}\right) + 2u_x \hat{\bar{\kappa}}_x^{'} - 2u_y \hat{\bar{\kappa}}_y^{'} + \frac{1}{2}(\hat{\sigma}_{xx}^{'} - \hat{\sigma}_{yy}^{'})\right\} + 3u_x \hat{h}_1 - 3u_y \hat{h}_2. \tag{A.10}$$

Clearly, a cascaded structure is already evident in the collision kernels of the second order moments, which is unlike that for the fluid flow LBE solver, where the cascaded structure starts to appear only at the third order moment collision kernels. This arises due to differences in the number of collision invariants between the two cascaded LBE models. Next, considering the post-collision state of the off-diagonal, second order central moment as

$$\begin{aligned} \hat{\kappa}_{xy}^{eq} = 0 &= \langle \overline{g}_\alpha^p | (e_{\alpha x} - u_x)(e_{\alpha y} - u_y) \rangle \\ &= \langle \overline{g}_\alpha^p | e_{\alpha x} e_{\alpha y} \rangle - u_y \langle \overline{g}_\alpha^p | e_{\alpha x} \rangle - u_x \langle \overline{g}_\alpha^p | e_{\alpha y} \rangle + u_x u_y \langle \overline{g}_\alpha^p | T \rangle. \end{aligned} \tag{A.11}$$

Using $\langle \overline{g}_\alpha^p | e_{\alpha x} e_{\alpha y} \rangle = \hat{\kappa}_{xy}^{eq} + 4\hat{h}_5 + \hat{\sigma}_{xy}^{'}$ in the above equation and simplifying it as a tentative expression for $\hat{h}_5$ and then applying the relaxation parameter λ_5 to those terms that are not yet in the post-collision states, we get

$$\begin{aligned} \hat{h}_5 &= \frac{\lambda_5}{4}\left\{-u_x u_y T - \hat{\bar{\kappa}}_{xy}^{'} + u_x \hat{\bar{\kappa}}_y^{'} + u_y \hat{\bar{\kappa}}_x^{'} + \frac{1}{2}\hat{\sigma}_{xy}^{'}\right\} \\ &\quad + \frac{3}{2}(u_x \hat{h}_2 + u_y \hat{h}_1). \end{aligned} \tag{A.12}$$

Now, consider the determination of the third order moment collision kernel. Setting tentatively

$$\hat{\kappa}_{xxy}^{eq} = 0 = \langle \overline{g}_\alpha^p | (e_{\alpha x} - u_x)^2 (e_{\alpha y} - u_y) \rangle, \tag{A.13}$$

$$\hat{\kappa}_{xyy}^{eq} = 0 = \langle \overline{g}_\alpha^p | (e_{\alpha x} - u_x)(e_{\alpha y} - u_y)^2 \rangle, \tag{A.14}$$

and using

$$\langle \overline{g}_\alpha^p | e_{\alpha x}^2 e_{\alpha y} \rangle = \hat{\bar{\kappa}}_{xxy}^{'} + 4\hat{h}_2 - 4\hat{h}_6 + \hat{\sigma}_{xxy}^{'},$$

$$\langle \overline{g}_\alpha^p | e_{\alpha x} e_{\alpha y}^2 \rangle = \hat{\bar{\kappa}}_{xyy}^{'} + 4\hat{h}_1 - 4\hat{h}_7 + \hat{\sigma}_{xyy}^{'},$$

in Eqs. (A.13) and (A.14), respectively, and simplifying to obtain the tentative expressions for $\hat{h}_6$ and $\hat{h}_7$, respectively, and applying relaxation parameters to terms that are not yet post-collision states we obtain

$$\begin{aligned} \hat{h}_6 &= \frac{\lambda_6}{4}\left\{-u_x^2 u_y T + \hat{\bar{\kappa}}_{xxy}^{'} - u_y \hat{\bar{\kappa}}_{xx}^{'} - 2u_x \hat{\bar{\kappa}}_{xy}^{'} + u_x^2 \hat{\bar{\kappa}}_y^{'} + 2u_x u_y \hat{\bar{\kappa}}_x^{'} + \frac{1}{2}\hat{\sigma}_{xxy}^{'}\right\} \\ &\quad + \frac{1}{2}(2\hat{h}_2 + 3u_x^2 \hat{h}_2) - \frac{1}{4}u_y(6\hat{h}_3 + 2\hat{h}_4) + 3u_x u_y \hat{h}_1 - 2u_x \hat{h}_5, \end{aligned} \tag{A.15}$$

$$\begin{aligned} \hat{h}_7 &= \frac{\lambda_7}{4}\left\{-u_x u_y^2 T + \hat{\bar{\kappa}}_{xyy}^{'} - u_x \hat{\bar{\kappa}}_{yy}^{'} - 2u_y \hat{\bar{\kappa}}_{xy}^{'} + 2u_x u_y \hat{\bar{\kappa}}_y^{'} + u_y^2 \hat{\bar{\kappa}}_x^{'} + \frac{1}{2}\hat{\sigma}_{xyy}\right\} \\ &\quad + \frac{1}{2}(2\hat{h}_1 + 3u_y^2 \hat{h}_1) - \frac{1}{4}u_x(6\hat{h}_3 - 2\hat{h}_4) + 3u_x u_y \hat{h}_2 - 2u_y \hat{h}_5. \end{aligned} \tag{A.16}$$

Finally, by tentatively setting the post-collision state of the fourth order central moment to its corresponding equilibrium state we have

$$\hat{\kappa}^{eq}_{xxyy} = \frac{1}{9}T = \langle \overline{g}^{p}_{\alpha} | (e_{\alpha x} - u_x)^2 (e_{\alpha y} - u_y^2) \rangle \tag{A.17}$$

and applying $\langle \overline{g}^{p}_{\alpha} | e^2_{\alpha x} e^2_{\alpha y} \rangle = \hat{\kappa}^{eq'}_{xxyy} + 8\hat{h}_3 + 4\hat{h}_8 + \hat{\sigma}'_{xxyy}$ then simplifying Eq. (A.17) and applying the relaxation parameter λ_8 to obtain

$$\begin{aligned}
\hat{h}_8 \;=\; & \frac{\lambda_8}{4}\Big\{\frac{1}{9}T - u_x^2 u_y^2 T - \hat{\kappa}'_{xxyy} + 2u_x \hat{\kappa}'_{xyy} + 2u_y \hat{\kappa}'_{xxy} - u_x^2 \hat{\kappa}'_{yy} - u_y^2 \hat{\kappa}'_{xx} \\
& - 4u_x u_y \hat{\kappa}'_{xy} + 2u_x u_y^2 \hat{\kappa}'_{x} + 2u_x^2 u_y \hat{\kappa}'_{y} + \frac{1}{2}\hat{\sigma}'_{xxyy}\Big\} + (2u_x + 3u_x u_y^2)\hat{h}_1 \\
& + (2u_y + 3u_x^2 u_y)\hat{h}_2 - \Big(2 + \frac{3}{2}u_x^2 + \frac{3}{2}u_y^2\Big)\hat{h}_3 + \frac{1}{2}(u_x^2 - u_y^2)\hat{h}_4 \\
& - 4u_x u_y \hat{h}_5 - 2u_y \hat{h}_6 - 2u_x \hat{h}_7.
\end{aligned} \tag{A.18}$$

Appendix B. Chapman–Enskog multiscale analysis of the thermal cascaded LBM

In this appendix, a Chapman–Enskog (C–E) analysis of the thermal cascaded LBE is presented and the results of the analysis provide the macroscopic emergent equations,viz., the convection–diffusion equation (CDE) with a source term given in Eq. (1) earlier. In this regard, we consider the strategy of rewriting the central moment LBM in terms of the relaxation to a generalized equilibrium in the rest frame of reference. To facilitate analysis and its establish consistency to the CDE, it is sufficient to consider terms only up to second order in Mach number in such an equivalent formulation (Asinari, 2008; Premnath and Banerjee, 2009). In this regard, we consider performing calculations in terms of various raw moments (designated with "prime symbols") with respect to the non-orthogonal moment basis vectors collected in the matrix $\mathscr{T}$ and given in Eq. (3).

First, the base raw moment equilibrium $\hat{\kappa}^{eq'}_{x^m y^n}$ can be obtained from the corresponding central moment equilibria $\hat{\kappa}^{eq}_{x^m y^n}$ given in equation Eq. (16). This reads as

$$\hat{\kappa}^{eq'}_{0} = T, \tag{B.1a}$$

$$\hat{\kappa}^{eq'}_{x} = u_x T, \tag{B.1b}$$

$$\hat{\kappa}^{eq'}_{y} = u_y T, \tag{B.1c}$$

$$\hat{\kappa}^{eq'}_{xx} = c_s^2 T + u_x^2 T, \tag{B.1d}$$

$$\hat{\kappa}^{eq'}_{yy} = c_s^2 T + u_y^2 T, \tag{B.1e}$$

$$\hat{\kappa}^{eq'}_{xy} = u_x u_y T, \tag{B.1f}$$

$$\hat{\kappa}^{eq'}_{xxy} = c_s^2 u_y T + u_x^2 u_y T, \tag{B.1g}$$

$$\hat{\kappa}^{eq'}_{xyy} = c_s^2 u_x T + u_y^2 u_x T, \tag{B.1h}$$

$$\hat{\kappa}^{eq'}_{xxyy} = c_s^4 T + c_s^2 (u_x^2 + u_y^2) T + u_x^2 u_y^2 T. \tag{B.1i}$$

Similarly, the raw moment for the source terms can be obtained from their corresponding central moments Eq. (17), which are presented in Eq. (19a). Now, for convenience, the various raw moments can be related to their corresponding states in the velocity space via the non-orthogonal transformation matrix $\mathscr{T}$. We now define raw moments of distribution functions (including the transformed one), equilibrium and sources for convenience as

$$\hat{\mathbf{g}} = \mathscr{T}\mathbf{g}, \quad \hat{\overline{\mathbf{g}}} = \mathscr{T}\overline{\mathbf{g}}, \quad \hat{\mathbf{g}}^{\mathbf{eq}} = \mathscr{T}\mathbf{g}^{eq}, \quad \hat{\mathbf{S}} = \mathscr{T}\mathbf{S}, \tag{B.2}$$

where

$$\begin{aligned}
\hat{\mathbf{g}} &= (\hat{g}_0, \hat{g}_1, \hat{g}_2, ..., \hat{g}_8)^{\dagger} \\
&= (\hat{\kappa}'_0, \hat{\kappa}'_x, \hat{\kappa}'_y, \hat{\kappa}'_{xx} + \hat{\kappa}'_{yy}, \hat{\kappa}'_{xx} - \hat{\kappa}'_{yy}, \hat{\kappa}'_{xy}, \hat{\kappa}'_{xxy}, \hat{\kappa}'_{xyy}, \hat{\kappa}'_{xxyy})^{\dagger}, \\
\hat{\overline{\mathbf{g}}} &= (\hat{\overline{g}}_0, \hat{\overline{g}}_1, \hat{\overline{g}}_2, ..., \hat{\overline{g}}_8)^{\dagger} \\
&= \Big(\hat{\overline{\kappa}}'_0, \hat{\overline{\kappa}}'_x, \hat{\overline{\kappa}}'_y, \hat{\overline{\kappa}}'_{xx} + \hat{\overline{\kappa}}'_{yy}, \hat{\overline{\kappa}}'_{xx} - \hat{\overline{\kappa}}'_{yy}, \hat{\overline{\kappa}}'_{xy}, \hat{\overline{\kappa}}'_{xxy}, \hat{\overline{\kappa}}'_{xyy}, \hat{\overline{\kappa}}'_{xxyy}\Big)^{\dagger}, \\
\hat{\mathbf{S}} &= (\hat{S}_0, \hat{S}_1, \hat{S}_2, ..., \hat{S}_8)^{\dagger} \\
&= (\hat{\sigma}'_0, \hat{\sigma}'_x, \hat{\sigma}'_y, \hat{\sigma}'_{xx} + \hat{\sigma}'_{yy}, \hat{\sigma}'_{xx} - \hat{\sigma}'_{yy}, \hat{\sigma}'_{xy}, \hat{\sigma}'_{xxy}, \hat{\sigma}'_{xyy}, \hat{\sigma}'_{xxyy})^{\dagger}.
\end{aligned}$$

In order to maintain flexibility in the specification of the transport coefficient (i.e. the thermal diffusivity) appearing in the emergent CDE, we specify the raw moment equilibrium $\hat{\mathbf{g}}^{eq}$ by augmenting the base moment equilibria given in Eq. (B.1) with an extended first order moment equilibria involving the components of the temperature gradients with an adjustable coefficient (designated as D below). That is

$$\hat{\mathbf{g}}^{eq} = \mathscr{T}\,\mathbf{g}^{eq}. \tag{B.3}$$

Here

$$\hat{\mathbf{g}}^{eq} = \hat{\mathbf{g}}^{eq(0)} + \hat{\mathbf{g}}^{eq(1)}. \tag{B.4}$$

where, $\hat{\mathbf{g}}^{eq(0)}$ and $\hat{\mathbf{g}}^{eq(1)}$ are the base and extended moment equilibria, respectively, and are given as follows:

$$\begin{aligned}\hat{\mathbf{g}}^{eq(0)} &= (\hat{g}_0^{eq(0)}, \hat{g}_1^{eq(0)}, ..., \hat{g}_8^{eq(0)})^{\dagger} \\ &= \left(\hat{\kappa}_0^{eq'}, \hat{\kappa}_x^{eq'}, \hat{\kappa}_y^{eq'}, \hat{\kappa}_{xx}^{eq'} + \hat{\kappa}_{yy}^{eq'}, \hat{\kappa}_{xx}^{eq'} - \hat{\kappa}_{yy}^{eq'}, \hat{\kappa}_{xy}^{eq'}, \hat{\kappa}_{xxy}^{eq'}, \hat{\kappa}_{xyy}^{eq'}, \hat{\kappa}_{xxyy}^{eq'}\right)^{\dagger}\end{aligned} \tag{B.5}$$

$$\hat{\mathbf{g}}^{eq(1)} = (\hat{g}_0^{eq(1)}, \hat{g}_1^{eq(1)}, \hat{g}_2^{eq(1)}, \hat{g}_3^{eq(1)}, ..., \hat{g}_8^{eq(1)})^{\dagger} = (0, c_s^2 D\partial_x T, c_s^2 D\partial_y T, 0, 0, 0, 0, 0)^{\dagger} \tag{B.6}$$

We can then rewrite post-collision state of the thermal cascaded LBE in Eq. (13) in terms of the following:

$$\overline{\mathbf{g}}^{p} = \overline{\mathbf{g}} + \mathscr{T}^{-1}\left[-\Lambda(\hat{\mathbf{g}} - \hat{\mathbf{g}}^{eq}) + \left(\mathscr{I} - \frac{1}{2}\Lambda\right)\hat{\mathbf{S}}\right], \tag{B.7}$$

where Λ is a diagonal collision matrix given by

$$\Lambda = diag(\lambda_0, \lambda_1, \lambda_2, \lambda_3, ..., \lambda_8). \tag{B.8}$$

Now, we apply a Chapman–Enskog multiscale analysis by expanding the raw moments $\hat{\mathbf{g}}$ and the time derivative in terms of a small perturbation parameter $\epsilon = \delta t$ (which will be set to 1 at the end of the analysis) using the following multi-scale expansions:

$$\hat{\mathbf{g}} = \sum_{n=0}^{\infty} \epsilon^n \hat{\mathbf{g}}^{(n)} = \hat{\mathbf{g}}^{(0)} + \epsilon\hat{\mathbf{g}}^{(1)} + \epsilon^2\hat{\mathbf{g}}^{(2)}, \tag{B.9a}$$

$$\hat{\mathbf{g}}^{eq} = \sum_{n=0}^{\infty} \epsilon^n \hat{\mathbf{g}}^{eq(n)} = \hat{\mathbf{g}}^{eq(0)} + \epsilon\hat{\mathbf{g}}^{eq(1)}, \tag{B.9b}$$

$$\partial_t = \sum_{n=0}^{\infty} \epsilon^n \partial_{t_n} = \partial_{t_0} + \epsilon\partial_{t_1} + \epsilon^2\partial_{t_2}, \quad \nabla = \epsilon\nabla. \tag{B.9c}$$

Notice that in the above we have used the moment equilibria $\hat{\mathbf{g}}^{eq}$ in terms of the sum of the base moment equilibria $\hat{\mathbf{g}}^{eq(0)}$ and the extended moment equilibria $\hat{\mathbf{g}}^{eq(1)}$. In addition, a Taylor expansion is used for the representation of the streaming operator, which is carried out in its natural velocity space:

$$\mathbf{g}(\vec{x} + \vec{e}_\alpha\epsilon, t + \epsilon) = \sum_{n=0}^{n} \frac{\epsilon^n}{n!}(\partial_t + \vec{e}_\alpha \cdot \vec{\nabla})^n \mathbf{g}(\vec{x}, t). \tag{B.10}$$

The resulting zeroth, first and second order equations are

$$O(\epsilon^0): \quad \hat{\mathbf{g}}^{(0)} = \hat{g}^{eq}, \tag{B.11a}$$

$$O(\epsilon^1): \quad (\partial_{t_0} + \widehat{E}_i\partial_i)\hat{\mathbf{g}}^{(0)} = -\Lambda[\hat{\mathbf{g}}^{(1)} - \hat{\mathbf{g}}^{eq(1)}] + \hat{\mathbf{S}}, \tag{B.11b}$$

$$O(\epsilon^2): \quad \partial_{t_1}\hat{\mathbf{g}}^{(0)} + (\partial_{t_0} + \widehat{E}_i\partial_i)\left[\mathscr{I} - \frac{\Lambda}{2}\right]\hat{\mathbf{g}}^{(1)} = -\Lambda\hat{\mathbf{g}}^{(2)}. \tag{B.11c}$$

where $\widehat{E}_i = \mathscr{T}(e_{\alpha i}\mathscr{I})\mathscr{T}^{-1}, \quad i \in x, y$. In to order derive the macroscopic CDE, up to the first order moment components in $O(\epsilon)$ (Eq. (B.11b)) are relevant, which are listed as follows:

$$\partial_{t_0} T + \partial_x(Tu_x) + \partial_y(Tu_y) = G, \tag{B.12a}$$

$$\partial_{t_0}(Tu_x) + \partial_x\left(\frac{1}{3}T + Tu_x^2\right) + \partial_y(Tu_x u_y) = -\lambda_1\hat{g}_1^{(1)} + \frac{1}{3}D\lambda_1\partial_x T + u_x G, \tag{B.12b}$$

$$\partial_{t_0}(Tu_y) + \partial_x(Tu_x u_y) + \partial_y\left(\frac{1}{3}T + Tu_y^2\right) = -\lambda_2\hat{g}_2^{(1)} + \frac{1}{3}D\lambda_2\partial_y T + u_y G, \tag{B.12c}$$

Similarly, the zeroth order moment component in Eq. (B.11c) is needed in deriving the CDE which reads as

$$\begin{aligned}\partial_{t_1} T &+ \partial_x\left[\left(1 - \frac{\lambda_1}{2}\right)\hat{g}_1^{(1)}\right] + \partial_y\left[\left(1 - \frac{\lambda_2}{2}\right)\hat{g}_2^{(1)}\right] \\ &+ \partial_x\left[\frac{\lambda_1}{6}D\partial_x T\right] + \partial_y\left[\frac{\lambda_2}{6}D\partial_y T\right] = 0.\end{aligned} \tag{B.13}$$

Now, combining Eqs. (B.12a) with ϵ times Eq. (B.13) and setting $\partial_t = \partial_{t_0} + \epsilon\partial_{t_1}$, we get the dynamical equations for the conserved moment after setting the parameter ϵ to unity. That is,

$$\partial_t T + \partial_x(Tu_x) + \partial_y(Tu_y) = -\epsilon\partial_x\left[\left(1-\frac{\lambda_1}{2}\right)\hat{g}_1^{(1)}\right] - \epsilon\partial_y\left[\left(1-\frac{\lambda_2}{2}\right)\hat{g}_2^{(1)}\right] - \epsilon\partial_x\left[\frac{\lambda_1}{6}D\partial_x T\right] - \epsilon\partial_y\left[\frac{\lambda_2}{6}D\partial_y T\right] + G. \tag{B.14}$$

In the above equation, Eq. (B.14), we need the first order non-equilibrium raw moments $\hat{g}_1^{(1)}$ and $\hat{g}_2^{(1)}$. They can be obtained from Eqs. (B.12b) and (B.12c), respectively. Thus,

$$\hat{g}_1^{(1)} = \frac{1}{\lambda_1}\left[-\partial_{t_0}(u_x T) - \partial_x\left(\frac{1}{3}T + u_x^2 T\right) - \partial_y(u_x u_y T) + u_x G\right] + \frac{1}{3}D\partial_x T, \tag{B.15}$$

$$\hat{g}_2^{(1)} = \frac{1}{\lambda_2}\left[-\partial_{t_0}(u_y T) - \partial_x(u_x u_y T) - \partial_y\left(\frac{1}{3}T + u_y^2 T\right) + u_y G\right] + \frac{1}{3}D\partial_y T. \tag{B.16}$$

The above equations can be simplified by considering the results from the C–E expansion of the cascaded LBM for fluid flow (NSE) (Premnath and Banerjee, 2009) and neglecting all terms of $O(u^2)$ and higher, which is sufficient to establish consistency with the CDE as the LBE are used for flow simulations in the incompressible limit. Thus, after some simplifications and rearrangements we get

$$\hat{g}_1^{(1)} \approx \frac{1}{3}\left\{D - \frac{1}{\lambda_1}\right\}\partial_x T, \tag{B.17}$$

$$\hat{g}_2^{(1)} \approx \frac{1}{3}\left\{D - \frac{1}{\lambda_2}\right\}\partial_y T. \tag{B.18}$$

Now, by substituting these simplified expressions for the non-equilibrium moments, Eqs. (B.17) and (B.18), into Eq. (B.14) it follows that

$$\partial_t T + \partial_x(Tu_x) + \partial_y(Tu_y) = \partial_x[\alpha_1\partial_x T] + \partial_y[\alpha_2\partial_y T] + G \tag{B.19}$$

which represents the convection–diffusion equation (CDE) with a source term. The coefficients α_1 and α_2 represent the thermal diffusivity and are related to their relaxation parameters λ_1 and λ_2 ,and the adjustable parameter D in the extended moment equilibria:

$$\alpha_1 = \frac{1}{3}\left(\frac{1}{\lambda_1} - \frac{1}{2} - D\right), \quad \alpha_2 = \frac{1}{3}\left(\frac{1}{\lambda_2} - \frac{1}{2} - D\right) \tag{B.20}$$

For isotropy of thermal diffusion, we have $\alpha = \alpha_1 = \alpha_2$, and it follows that $\lambda_1 = \lambda_2$, and the rest of the higher order relaxation parameters can be tuned to improve the numerical stability. Finally, the temperature gradients $\partial_x T$ and $\partial_y T$ needed in the extended moment equilibria Eq. (B.6) can be computed locally from Eqs. (B.17) and (B.18), i.e. the first order non-equilibrium moments. Using $\hat{g}_1^{(1)} = \hat{g}_1 - \hat{g}_1^{eq(0)} = \hat{\hat{\kappa}}_x^{'} - \hat{\kappa}_x^{eq'}$ and $\hat{g}_2^{(1)} = \hat{g}_2 - \hat{g}_2^{eq(0)} = \hat{\hat{\kappa}}_y^{'} - \hat{\kappa}_y^{eq'}$ in Eqs. (B.17) and (B.18), and rearranging, we get

$$\partial_x T = \frac{3\lambda_1\left(\hat{\hat{\kappa}}_x^{'} - \hat{\kappa}_x^{eq'}\right)}{(D\lambda_1 - 1)}, \tag{B.21a}$$

$$\partial_y T = \frac{3\lambda_2\left(\hat{\hat{\kappa}}_y^{'} - \hat{\kappa}_y^{eq'}\right)}{(D\lambda_2 - 1)} \tag{B.21b}$$

where $\hat{\kappa}_x^{'eq} = u_x T$, and $\hat{\kappa}_y^{'eq} = u_y T$.

References

Aidun, C.K., Clausen, J.R., 2010. Lattice Boltzmann method for complex flows. Annu. Rev. Fluid Mech. 42, 439–472.

Alexander, F.J., Chen, S., Sterling, J., 1993. Lattice Boltzmann thermohydrodynamics. Phys. Rev. E 47 (4), R2249.

Asinari, P., 2008. Generalized local equilibrium in the cascaded lattice Boltzmann method. Phys. Rev. E 78 (1), 016701.

Chai, Z., Zhao, T., 2013. Lattice Boltzmann model for the convection–diffusion equation. Phys. Rev. E 87 (6), 063309.

Chai, Z., Zhao, T., 2014. Nonequilibrium scheme for computing the flux of the convection–diffusion equation in the framework of the lattice Boltzmann method. Phys. Rev. E 90 (1), 013305.

Chen, S., Doolen, G.D., 1998. Lattice Boltzmann method for fluid flows. Annu. Rev. Fluid Mech. 30 (1), 329–364.

Chopard, B., Falcone, J., Latt, J., 2009. The lattice Boltzmann advection–diffusion model revisited. Eur. Phys. J. – Special Top. 171 (1), 245–249.

Dixit, H., Babu, V., 2006. Simulation of high Rayleigh number natural convection in a square cavity using the lattice Boltzmann method. Int. J. Heat Mass Transf. 49 (3), 727–739.

Gan, Y., Xu, A., Zhang, G., Li, Y., 2011. Lattice Boltzmann study on Kelvin–Helmholtz instability: roles of velocity and density gradients. Phys. Rev. E 83 (5), 056704.

Geier, M., Greiner, A., Korvink, J.G., 2006. Cascaded digital lattice Boltzmann automata for high Reynolds number flow. Phys. Rev. E 73 (6), 066705.

Geier, M., Schönherr, M., Pasquali, A., Krafczyk, M., 2015. The cumulant lattice Boltzmann equation in three dimensions: theory and validation. Comput. Math. Appl. 70 (4), 507–547.

Ginzburg, I., 2005. Equilibrium-type and link-type lattice Boltzmann models for generic advection and anisotropic-dispersion equation. Adv. Water Resour. 28 (11), 1171–1195.

Ginzburg, I., 2013. Multiple anisotropic collisions for advection–diffusion lattice Boltzmann schemes. Adv. Water Resour. 51, 381–404.

Guo, Z., Shi, B., Zheng, C., 2002. A coupled lattice bgk model for the Boussinesq equations. Int. J. Numer. Methods Fluids 39 (4), 325–342.

Guo, Z., Shu, C., 2013. Lattice Boltzmann Method and its Applications in Engineering. vol. 3 World Scientific.

Guo, Z., Zheng, C., Shi, B., Zhao, T., 2007. Thermal lattice Boltzmann equation for low mach number flows: decoupling model. Phys. Rev. E 75 (3), 036704.

Hajabdollahi, F., Premnath, K.N., 2017. Improving the low Mach number steady state convergence of the cascaded lattice Boltzmann method by preconditioning. Comput. Math. Appl.

Hajabdollahi, F., Premnath, K.N., 2018. Central moments-based cascaded lattice Boltzmann method for thermal convective flows in three-dimensions. Int. J. Heat Mass Transf. 120, 838–850.

He, X., Chen, S., Zhang, R., 1999. A lattice Boltzmann scheme for incompressible multiphase flow and its application in simulation of Rayleigh–Taylor instability. J. Comput. Phys. 152 (2), 642–663.

He, X., Shan, X., Doolen, G.D., 1998. Discrete Boltzmann equation model for nonideal gases. Phys. Rev. E 57 (1), R13.

Hortmann, M., Perić, M., Scheuerer, G., 1990. Finite volume multigrid prediction of laminar natural convection: bench-mark solutions. Int. J. Numer. Methods Fluids 11 (2), 189–207.
Huang, J., Yong, W.-A., 2015. Boundary conditions of the lattice Boltzmann method for convection–diffusion equations. J. Comput. Phys. 300, 70–91.
Khazaeli, R., Mortazavi, S., Ashrafizaadeh, M., 2013. Application of a ghost fluid approach for a thermal lattice Boltzmann method. J. Comput. Phys. 250, 126–140.
Krüger, T., Kusumaatmaja, H., Kuzmin, A., Shardt, O., Silva, G., Viggen, E.M., 2017. The Lattice Boltzmann Method. Springer.
Lallemand, P., Luo, L.-S., 2003. Hybrid finite-difference thermal lattice Boltzmann equation. Int. J. Mod. Phys. B 17 (01n02), 41–47.
Li, L., Mei, R., Klausner, J.F., 2013. Boundary conditions for thermal lattice Boltzmann equation method. J. Comput. Phys. 237, 366–395.
Li, Q., Luo, K., He, Y., Gao, Y., Tao, W., 2012. Coupling lattice Boltzmann model for simulation of thermal flows on standard lattices. Phys. Rev. E 85 (1), 016710.
Mai, H.-C., Lin, K.-H., Yang, C.-H., Lin, C.-A., 2010. A thermal lattice Boltzmann model for flows with viscous heat dissipation. Comput. Model. Eng. Sci. 61 (1), 45–62.
Meng, X., Guo, Z., 2015. Multiple-relaxation-time lattice Boltzmann model for incompressible miscible flow with large viscosity ratio and high Péclet number. Phys. Rev. E 92 (4), 043305.
Mezrhab, A., Bouzidi, M., Lallemand, P., 2004. Hybrid lattice-boltzmann finite-difference simulation of convective flows. Comput. Fluids 33 (4), 623–641.
Ning, Y., Premnath, K.N., Patil, D.V., 2016. Numerical study of the properties of the central moment lattice Boltzmann method. Int. J. Numer Methods Fluids 82 (2), 59–90.
Ponce Dawson, S., Chen, S., Doolen, G.D., 1993. Lattice Boltzmann computations for reaction–diffusion equations. J. Chem. Phys. 98 (2), 1514–1523.
Premnath, K.N., Banerjee, S., 2009. Incorporating forcing terms in cascaded lattice Boltzmann approach by method of central moments. Phys. Rev. E 80 (3), 036702.
Rasin, I., Succi, S., Miller, W., 2005. A multi-relaxation lattice kinetic method for passive scalar diffusion. J. Comput. Phys. 206 (2), 453–462.
Shi, Y., Zhao, T., Guo, Z., 2004. Thermal lattice Bhatnagar–Gross–Krook model for flows with viscous heat dissipation in the incompressible limit. Phys. Rev. E 70 (6), 066310.
Van der Sman, R., Ernst, M., 2000. Convection–diffusion lattice Boltzmann scheme for irregular lattices. J. Comput. Phys. 160 (2), 766–782.
Succi, S., 2001. The Lattice Boltzmann Equation for Fluid Dynamics and Beyond. Clarendon Press, Oxford.
de Vahl Davis, G., 1983. Natural convection of air in a square cavity: a bench mark numerical solution. Int. J. Numer. Methods Fluids 3 (3), 249–264.
Wang, J., Wang, D., Lallemand, P., Luo, L.-S., 2013. Lattice Boltzmann simulations of thermal convective flows in two dimensions. Comput. Math. Appl. 65 (2), 262–286.
Yoshida, H., Nagaoka, M., 2010. Multiple-relaxation-time lattice Boltzmann model for the convection and anisotropic diffusion equation. J. Comput. Phys. 229 (20), 7774–7795.
Zhang, T., Shi, B., Guo, Z., Chai, Z., Lu, J., 2012. General bounce-back scheme for concentration boundary condition in the lattice-Boltzmann method. Phys. Rev. E 85 (1), 016701.